

Synthesis and Single-Molecule Force Spectroscopy of Supramolecular Capsules

Dissertation

Tobias Schröder

Department of Chemistry
Department of Physics
University of Bielefeld
2010

Erklärung

Hiermit erkläre ich an Eides statt, dass ich die vorliegende Arbeit selbstständig und ohne unerlaubte Hilfe angefertigt habe und dabei keine als die angegebenen Hilfsmittel verwendet habe.

Mit einer Auslegung in der Universitätsbibliothek bin ich einverstanden.

Diese Arbeit ist auf alterungsbeständigem Papier gemäß ISO 9706 gedruckt.

Bielefeld im März 2010.

(Tobias Schröder)

Diese Arbeit entstand unter der Leitung von

Prof. Dr. Jochen Mattay

in der Arbeitsgruppe Organische Chemie I

und

Prof. Dr. Dario Anselmetti

in der Arbeitsgruppe Experimentelle Biophysik und Angewandte Nanowissenschaften

in der Fakultät für Chemie und der Fakultät für Physik der Universität Bielefeld im Rahmen des Sonderforschungsbereichs 613 der DFG.

Danksagung

Interdisziplinäre Forschungsprojekte wie dieses leben von der intensiven Zusammenarbeit der beteiligten Arbeitsgruppen. Mein herzlicher Dank gilt Prof. Dr. Dario Anselmetti und Prof. Dr. Jochen Mattay, unter deren hervorragender Anleitung ich diese Arbeit durchgeführt habe. Mit besonderer Offenheit für die unterschiedlichen Herangehensweisen der Fachrichtungen und großem Vertrauen in meine Arbeit haben Sie mich gefordert, unterstützt und meinen Blickwinkel erweitert. Mit Ihrem Enthusiasmus, Verbindlichkeit und Humor haben sie eine angenehme Arbeitsatmosphäre geschaffen, die zum Erfolg des Forschungsprojekts wesentlich beigetragen hat.

Die vielfältige Aufgabenstellung erforderte Know-how in chemischen und physikalischen Fragen. Für die umfangreiche Unterstützung bei den physikalischen Untersuchungen und die herzliche Aufnahme danke ich besonders dem Arbeitskreis für Angewandte Nanowissenschaften und Biophysik. Hervorheben möchte ich dabei Dr. Volker Walhorn, Dipl.-Phys. Alexander Harder und Dipl.-Biochem. Daniel Wesner, die mir bei der Bedienung der Geräte und der Auswertung der Daten zur Seite gestanden haben. Dipl.-Ing. Christoph Pelargus danke ich für die instrumentelle Unterstützung und Modifikationen der Setups. Für die Hilfe bei der Charakterisierung von Oberflächen durch Fluoreszenzaufnahmen danke ich Dipl.-Phys. Thorsten Bergmann. Auch den ehemaligen Mitgliedern des Arbeitskreises, Prof. Dr. Robert Ros und Dipl.-Phys. Alexander Fuhrmann möchte ich für die Unterstützung zu Dank verpflichtet. Bei Dr. Katja Tönsing und Gabi Krome bedanke ich mich für Ihre Hilfe in allen organisatorischen Belangen.

Besonderer Dank gilt auch den derzeitigen und ehemaligen Mitgliedern des Arbeitskreises für Organische Chemie I für die Diskussionen von Synthesen und Arbeitstechniken, die praktische Hilfe im Laboralltag, die freundschaftliche Arbeitsatmosphäre und zahlreiche Aktivitäten außerhalb der Universität. Für besonders engagierte und kompetente Hilfe bei der Synthese und bei technischen (sowie eigentlich allen anderen) Fragestellungen danke ich Thomas Geisler. Ebenso möchte ich Dieter Barth für technische und praktische Unterstützung danken. Prof. Dr. Dietmar Kuck danke ich für Diskussionsbeiträge zur Synthesestrategie. Arja Gaestel danke ich für die schnelle und zuverlässige Bearbeitung organisatorischer Aufgaben. Für die optimale Versorgung mit Chemikalien und die schnelle Beschaffung von Materialien danke ich dem Chemikalienlager, insbesondere Heike Kosellek und Stefanie Boese.

Bei der Untersuchung von Koordinationskäfigen und der Charakterisierung von allen möglichen und unmöglichen Syntheseprodukten haben die analytischen Abteilungen (NMR-Messungen: Peter Mester, Dr. Andreas Mix; Massenspektrometrie: Dr. Matthias C. Letzel, Dipl.-Ing. Oliver Kollas und Sandra Heidtkamp, Elementaranalytik: Brigitte Michel) gute Arbeit geleistet. Vielen Dank!

Dr. Ralf Brodbeck danke ich für wissenschaftliche Diskussionen, die Berechnung der Struktur des Koordinationskäfigs und die Hilfe bei der Erstellung der Abbildungen. Diese Arbeiten haben Strukturen vorstellbar gemacht und gleichzeitig die Phantasie beflügelt!

Prof. Dr. Dirk Volkmer, Dr. Markus Tonigold und Dr. Junmin Liu danke ich für die Durchführung der SAXS-Messungen und die produktive Kooperation.

Meinen Forschungspraktikanten B.Sc. Michaela Klaß, Anna Reimer und Marcel Heidlindemann danke ich für Ihre engagierte Mitarbeit. Sie haben Ihre Teilprojekte mit großem Einsatz verfolgt und ihren Teil zum Gelingen dieser Arbeit beigetragen.

Außerhalb der Universität hat mich in der Zeit meiner Promotion vor allem meine Birte unterstützt, bestärkt und mir immer wieder Kraft gegeben. „Danke“ ist dafür noch viel zu wenig!

Contents

1	Introduction	1
2	Structures of Supramolecular Capsules	3
2.1	Cavitands and Calix[n]arenes: Building Blocks for Supramolecular Capsules.....	3
2.2	Hydrogen-bonded Supramolecular Capsules based on Cavitands and Calix[n]arenes.....	5
2.3	Coordination Cages: Influence of Ligand Design on Metal-directed Self-Assembly.....	8
2.4	Terpyridines as Building Blocks for Coordination Cages.....	13
2.5	Objective.....	17
2.6	Results: Synthesis of a Large Metallosupramolecular Cage.....	18
3	Dynamics and Stability of Hydrogen-bonded Supramolecular Capsules	25
3.1	Self-Assembly Dynamics of Supramolecular Capsules.....	25
3.2	Atomic-Force Single-Molecule Force Spectroscopy (AFM-SMFS).....	28
3.3	Single-Molecule Force Spectroscopy of Hydrogen-bonded Supramolecular Systems.....	34
3.4	Objective.....	38
3.5	Results.....	40
3.5.1	Immobilization of the Building Blocks.....	40
3.5.2	Single-Molecule Force Spectroscopy of Supramolecular Capsules....	46
4	Summary	50
5	References	55

6 Appendix 60
6.1 Glossary..... 60
6.2 List of Original Publications..... 61

1 Introduction

Concepts of supramolecular chemistry have changed the way scientists perceive chemical structures: not as independent entities, but as interacting structures. The “chemistry beyond the molecule” has opened the view to understand, design and use assemblies of molecules.¹ Starting with the development of ligand-receptor systems to explore the basic principles of molecular recognition, the increasing systematization of supramolecular binding motifs and building blocks facilitated the self-assembly by design, yielding impressive architectures and stimulating chemistry, biology, physics and material sciences.² The wide implementation is reflected in the research areas, such as supramolecular catalysis,³ supramolecular polymers,⁴ and supramolecular electronics.⁵ Adaptive chemical systems, which can be obtained taking advantage of the weakness of supramolecular bonds and the reversibility of the formation of supramolecular structures, are subject of current research interest.⁶ Besides exploring the prospects offered by supramolecular chemistry in various fields, a deeper understanding of its principles remains a basic challenge. Two important aspects are the controlled self-assembly of hollow architectures and the dynamic strength of interactions between building blocks.

The inner cavity of supramolecular capsules provides a discrete, well-defined environment ideally suited to investigate effects of compartmentalization and processes in confined spaces.⁷ To realize technical applications as detection and stabilization of encapsulated molecules or their use as nano-sized reaction vessels, precise control of important factors as size, stability, porosity of the walls and functionalization of the inner surface have to be achieved.⁸⁻¹⁰ Several capsules have been synthesized and a proof of principle for several applications have been provided, but in most cases their use is restricted to small guest molecules. The development of spacious architectures which are able to encapsulate several bulky molecules and amenable for a decoration of the inner surface with functional groups will constitute an important step on the way to functional systems.

The stability of supramolecular binding motifs defines the degree of reversibility during self-assembly and therefore the ability for self-correction, ensures the integrity of the structure and controls the adaptability to environmental changes.² Connecting building blocks *via* multiple hydrogen bonds is one of the most frequently used strategies to obtain dynamic structures. The combination of predictable orientation and fast equilibration accounts for the high attractivity of employing hydrogen bonds in supramolecular design principles.¹¹

Several capsules based on hydrogen bond motifs have been synthesized, with dimeric systems built up from functionalized cavitands as one important subgroup.⁸ The uniform design defined by the cavitands makes these structures valuable objects for the study of different bridging units. Atomic force single-molecule force spectroscopy (AFM-SMFS) represents an outstanding technique providing quantitative data on mechanical stabilities of interactions and mechanochemical effects.¹²⁻¹⁵ Moreover, detailed information about the energy landscape of interactions as well as quantitative kinetic and thermodynamic data can be obtained.¹⁶⁻¹⁸ Therefore, single-molecule force spectroscopy is a unique tool bridging the molecular and the macroscopic world and is especially suited for the characterization of supramolecular binding motifs in different dimensions to understand interactions at the single-molecule level.

2 Structures of Supramolecular Capsules

2.1 Cavitands and Calix[n]arenes: Building Blocks for Supramolecular Capsules

The synthesis of hollow architectures based on cavitands started in 1985, when CRAM *et al.* reported on the inclusion of solvent molecules in a carcerand obtained by covalent linkage of two cavitands.¹⁹ Since then, molecular and supramolecular capsules have been prepared from cavitands and calix[n]arenes due to two important properties: the bowl-shaped form and the various functionalizations which can be introduced at the *upper rim* of the cavitands or the *wider rim* of the calix[n]arenes (Figure 1).

While the conformation of the methylene-bridged cavitands **1** is fixed (Figure 1 a), a number of more flexible cavitands with other bridging units (BU) have been prepared (Figure 1 b).²⁰ Depending on the substituent R' at phenolic oxygen and the group (G) attached to the *wider rim*, the calix[n]arenes **2** can adopt different conformations (Figure 1 c and 1 d).^{21,22} The calix[n]arenes with more than four phenol units in the cyclophane basis are particularly flexible.

Because cavitands and calix[n]arenes with various functional groups (G) can be synthesized, a range of reactions can be applied to obtain substituted derivatives. Some of these molecules can be used as receptors for neutral molecules and ions, for the synthesis of stationary phases for chromatography and as catalysts for organic reactions.^{22,23} In the following sections it will be shown, that cavitands and calix[n]arenes are valuable building blocks for complex structures as supramolecular capsules due to the unique combination of shape and functional groups that can be attached to the cyclophane basis.

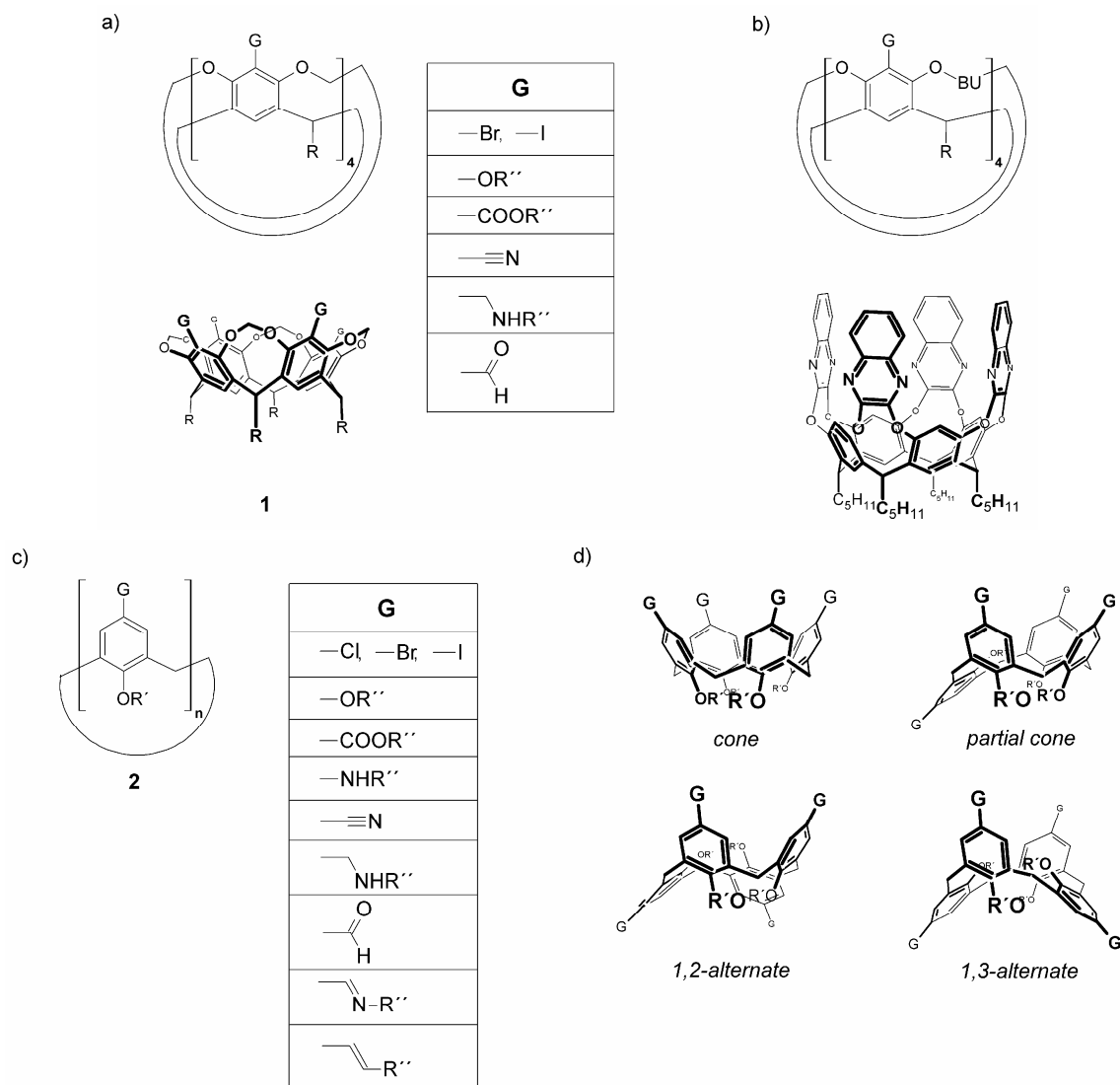


Figure 1: (a) Structure of a methylene-bridged calixarene **1** substituted with functional groups (G) at the *upper rim*. (b) General structure of calixarenes with different bridging units (BU) and one example of an aryl-bridged calixarene.²⁴ (c) Structure of calix[n]arenes **2** with functional groups (G) at the *wider rim*. (d) Conformations of calix[4]arenes.

2.2 Hydrogen-bonded Supramolecular Capsules based on Cavitanths and Calix[n]arenes

Following their covalent analogues, hydrogen-bonded supramolecular capsules have been synthesized from cavitands and calix[n]arenes.⁸ The heterodimeric aggregate **5** introduced by KOBAYASHI *et al.* shown in Figure 2 is a structurally well studied example for a hydrogen-bonded complex.²⁵ In solvents suited as guest molecules or in the presence of added guests, cavitands with four carboxylic acid groups and cavitands with four pyridyl groups selectively form heterodimers stitched together by four hydrogen bonds. In CDCl₃ (which is an ill-fitting guest), from a mixture of arenes selected 1,4-disubstituted benzenes were preferentially encapsulated (Figure 2 d).²⁶ This selectivity was attributed to specific host-guest interactions that stabilize the complex in addition to the hydrogen-bonding. One factor is the CH-halogen interactions between the *inner* protons of the methylene-bridges of the cavitand units and the halogen atom of an arylhalogenide guest. In the case of methoxy-substituted benzene guest molecules, the CH- π -interaction between the aromatic cavities of the cavitands and the polarized methoxy protons has a stabilizing effect. Independent from the functional groups, the filling of the void space inside the capsule by a guest of optimal size and shape has an important impact on capsule formation.

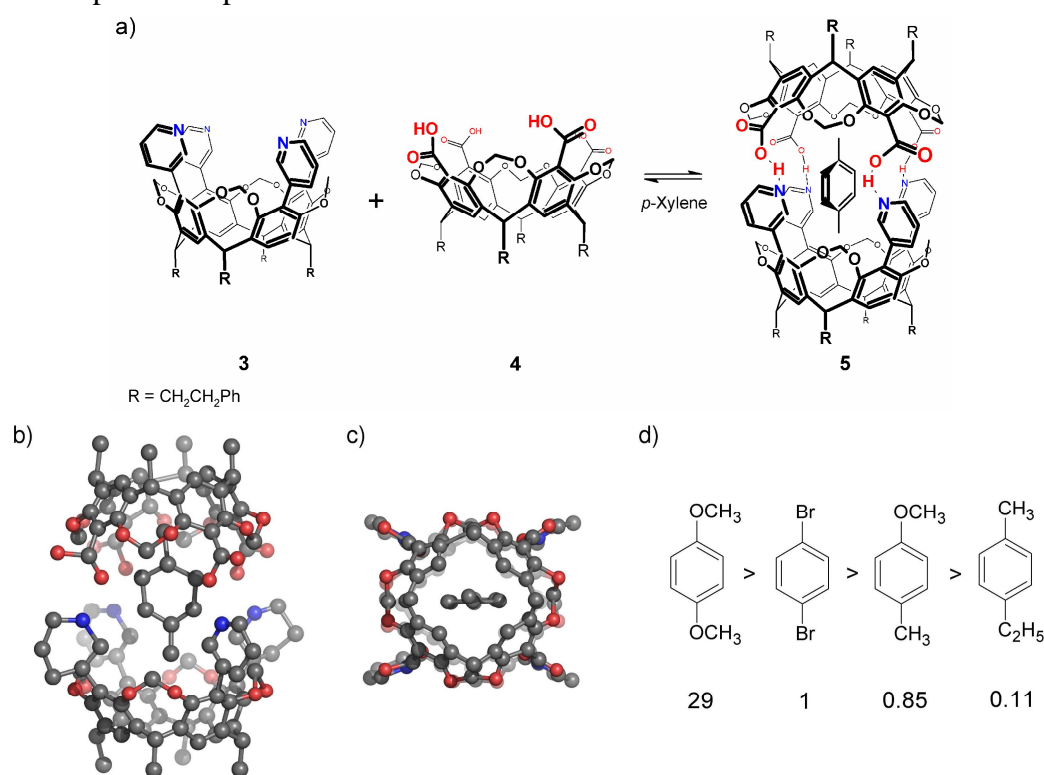


Figure 2: (a) Association of cavitands to the heterodimeric capsule **5** in *para*-xylene. (b), (c) Molecular structure of **5** (with one molecule *para*-xylene encapsulated) in the solid state as determined by X-ray diffraction analysis ((b) side view, (c) top view, alkyl chains omitted). (d) Preference of guest encapsulation of 1,4-disubstituted benzenes relative to 1,4-dibromobenzene determined by ¹H-NMR spectroscopy.

Dimeric hydrogen bonded capsules have also been obtained from calix[4]arenes (Figure 3). The tetra(urea)calix[4]arene **6** exists as a monomeric species in the *cone* conformation in polar solvents as DMSO.²⁷ In apolar solvents that are suited for encapsulation (as benzene and chloroform), the molecules form dimers **7** that are held together by hydrogen bonds between the HN- and the O=C- functions of the urea groups.^{27,28} Because no additional molecules take part in the hydrogen-bonding network, the building blocks are called “self-complementary”.

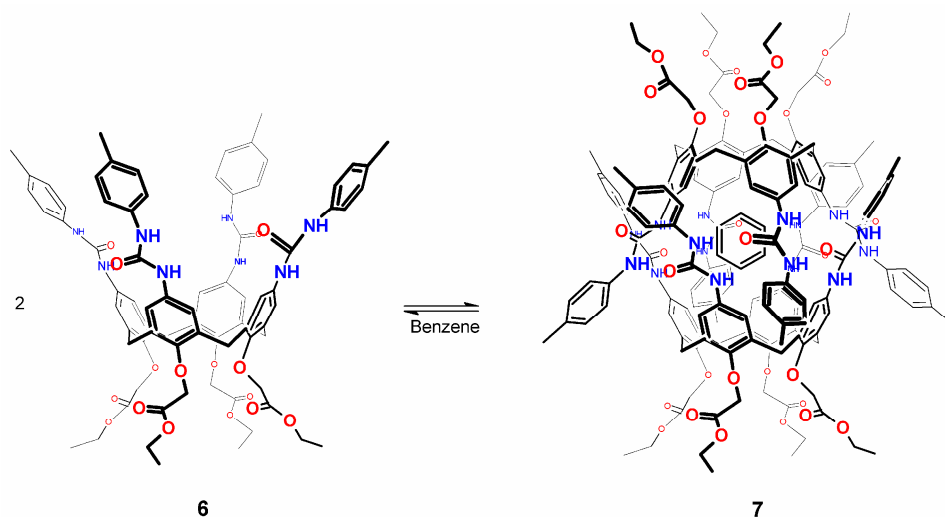


Figure 3: Association of the tetra(urea)calix[4]arene **6**.

The association of the tetra(urea)calix[4]arenes strongly depends on the substituents at the urea groups (Figure 4 a).²⁷ When two solutions of the dimer of the aryl-substituted tetra(urea)calix[4]arene **8** and the dimers of the sulfonyl-substituted tetra(urea)calix[4]arene **9** are combined, the mixed dimer **10** is formed quantitatively.²⁹ Covalent linkage of two tetra(urea)calix[4]arenes at the *narrow rim* yields compounds **11** – **13**, which exist as supramolecular polymers in apolar solvents (Figure 4 b and 4 c).³⁰ By addition of the calix[4]arenes **8** and **9** the aggregation to these “polycaps” can be controlled, because they serve as “endcaps” resulting in an effective depolymerization. Therefore, the polymerization can be switched off with **8**, **9** or polar and protic solvents.

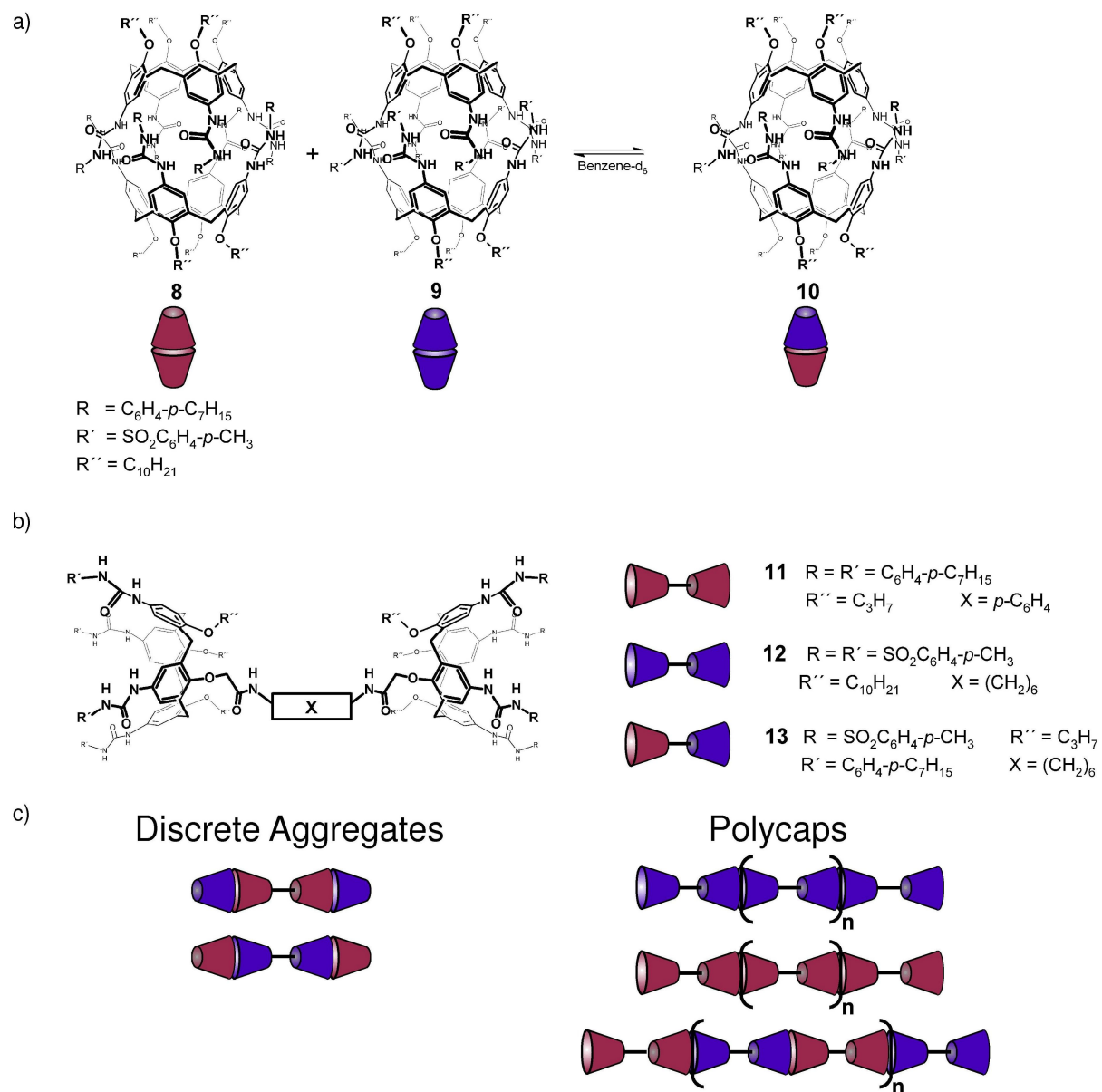


Figure 4: Formation of mixed dimeric capsules and supramolecular polymers based on aryl- and sulfonyl-substituted tetra(urea)calix[4]arenes.

2.3 Coordination Cages: Influence of Ligand Design on Metal-directed Self-Assembly

Several metallocupramolecular cages with different geometries have been synthesized from cavitands and calix[n]arenes functionalized with metal-coordinating groups at the *upper rim*.¹⁰ The successful self-assembly of such building blocks is a complex reaction, that yields the most thermodynamically stable product.³¹ A reversible formation of the coordinative bonds is necessary to allow “error correction” by partial disassembly of less stable intermediates to form the final assembly. On the other hand, a stable connection of the cages’ subunits has to be realized to ensure the integrity of the structure and allow the characterization of the assembly in solution. The development of rigid ligands with a high preference to self-assemble to only one aggregate with defined geometry is of major importance for the synthesis of coordination cages. The degree of preorganization of building blocks derived from cavitands and calix[n]arenes is controlled by the shape and conformational freedom of the cavitand or calix[n]arene basis and the flexibility of the attachment of the metal-coordinating group. To illustrate the impact of the ligand properties on the geometry of the obtained structures, selected examples of coordination cages based on cavitands are presented in this chapter.

The self-assembly of the tetra(cyano)cavitands **14** and **15** with a different flexibility of the cavitand basis was investigated by DALCANALE *et al.* (Figure 5).³² Compared to the methylene bridged cavitand **15**, the ethylene bridged cavitand **14** is conformationally less rigid. The higher flexibility of **14** accounts for the lower tendency to aggregate to discrete coordination cages. While **15** forms dimeric coordination cages in the presence of Pd(dppp)(CF₃SO₃)₂, no successful capsule self-assembly was observed for the flexible cavitand **14**.

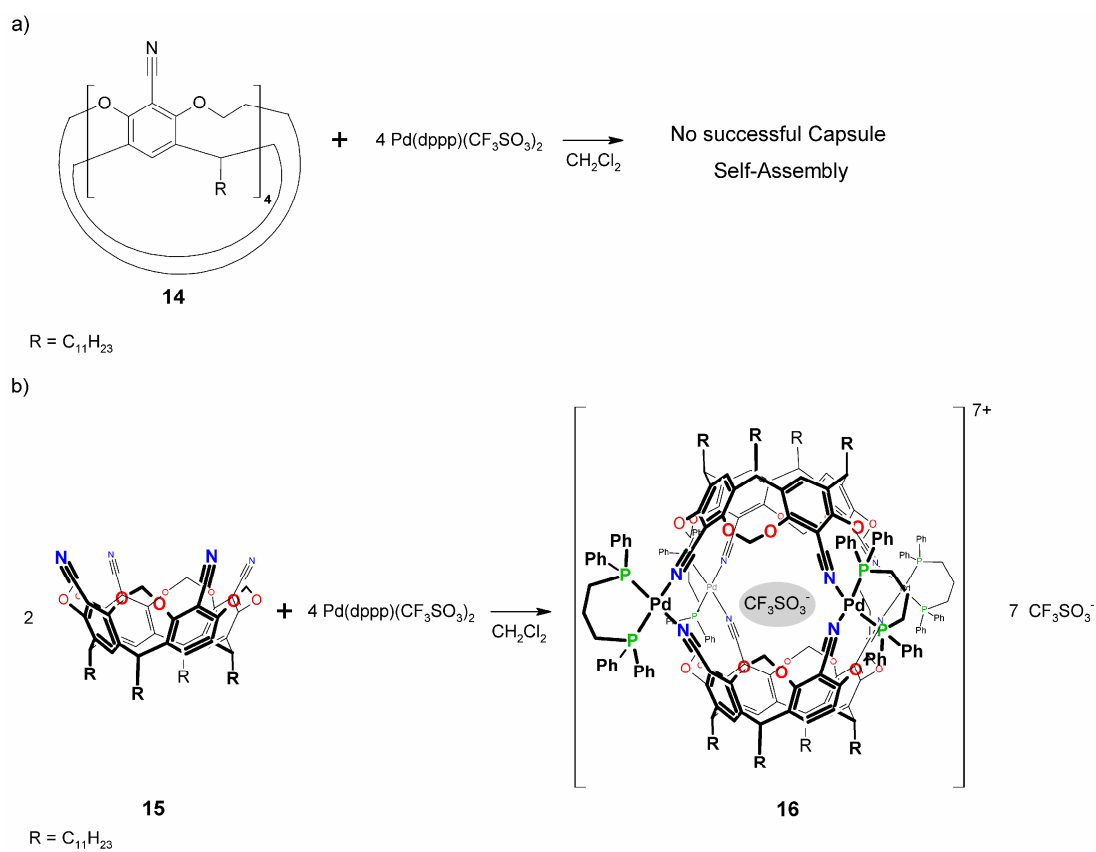


Figure 5: (a) The ethylene-bridged cavitant **14** is not suited for capsule self-assembly with $Pd(dppp)(CF_3SO_3)_2$.
(b) Self-assembly of the methylene-bridged cavitant **15**.

The kind of attachment of the metal coordinating groups to the cavitand is an important structure-defining parameter. HONG *et al.* studied the self-assembly of a cavitand **17** functionalized with pyridyl groups *via* flexible ether linkages (Figure 6).³³ Due to the conformational freedom of the connection, intramolecular coordination of the Pt²⁺ centers is observed in competition with intermolecular complexation leading to the supramolecular capsule **18**. While the capsule **18** and the half-capsule **19** are in dynamic equilibrium in nitromethane, the dimeric capsule is formed exclusively in chloroform/methanol mixtures.

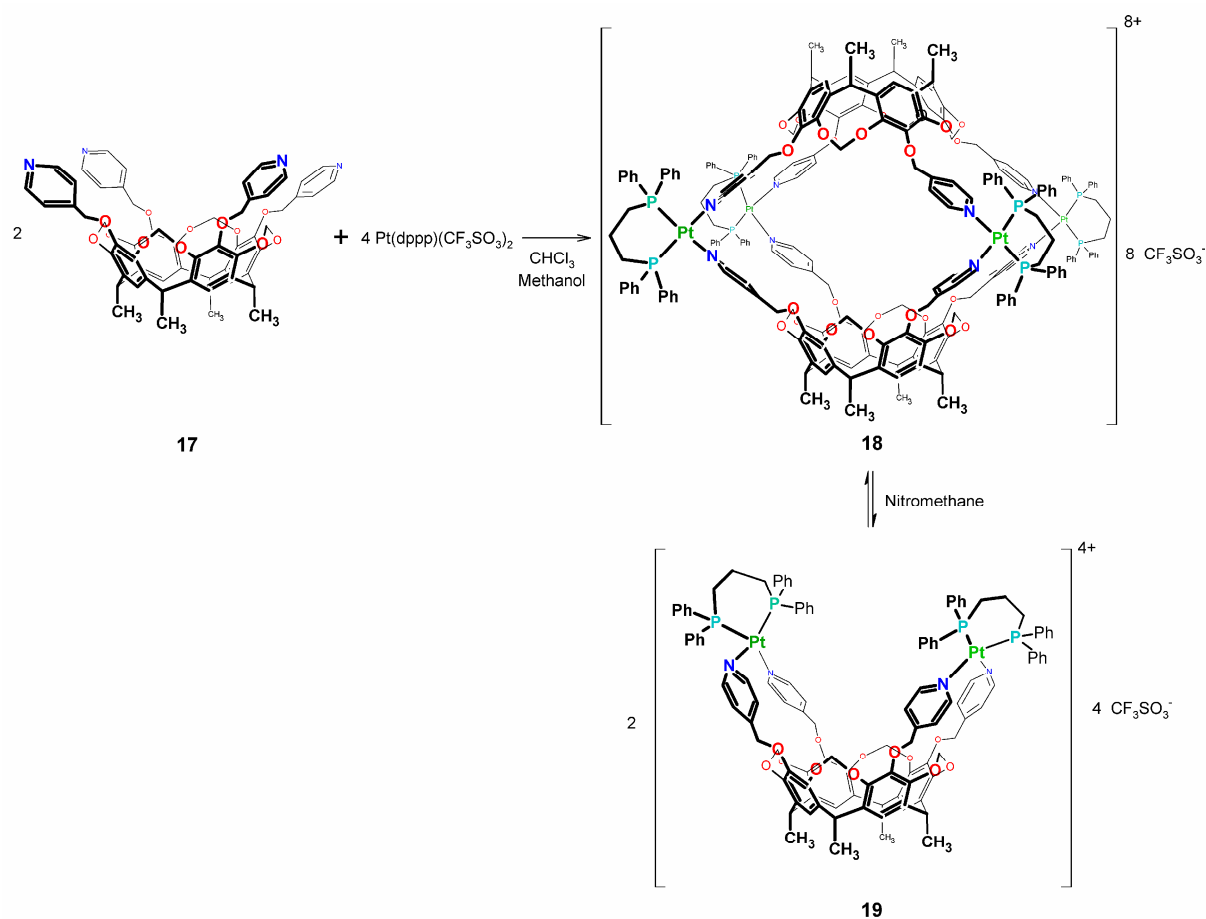


Figure 6: Self-assembly of **17** and equilibrium between capsule **18** and interclipped bowl **19**.

Further examples for structural diversity induced by non-rigid linkage of the metal coordinating groups to the cavitand basis have been provided by BEER *et al.* (Figure 7).³⁴ In the presence of different metal ions, the cavitand **21** with four thiocarbamate units attached *via* methylene groups to the cyclophane aggregates to trimeric or tetrameric species. Reaction of **21** with Zn^{2+} yields the trimeric aggregate **22** with the cavitands located at the corners of an equilateral triangle.³⁵ All edges of the triangle are doubly spanned by two zinc ions coordinated to the same cavitands. In the presence of Cu^{2+} ions, tetrameric species **23** are formed.³⁶ Determination of the molecular structure by X-ray diffraction analysis showed that the cavitands lie at the apices of a flattened tetrahedron with two edges doubly spanned by two copper ions coordinated to the same cavitands.

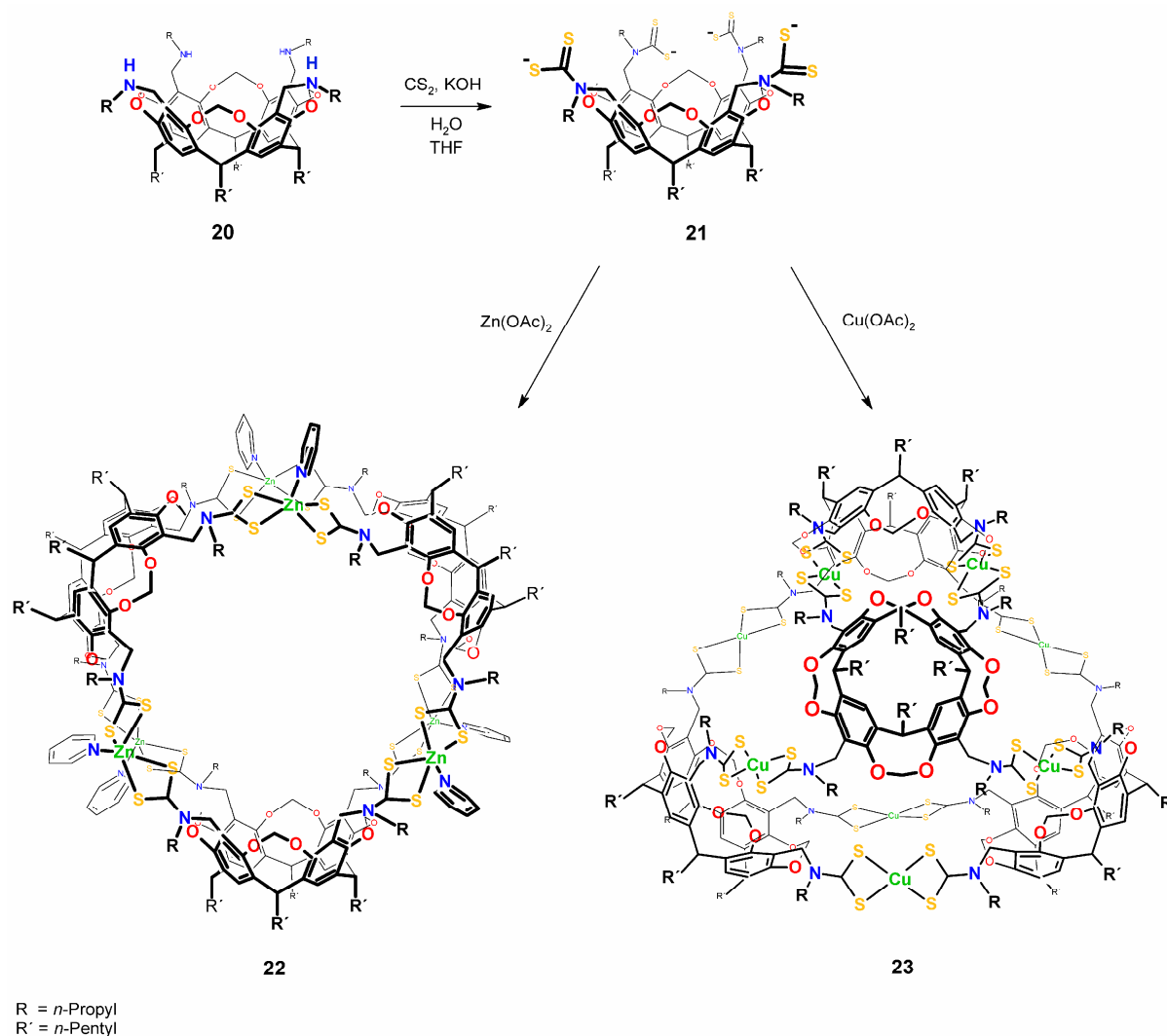


Figure 7: Synthesis of the tetra(thiocarbamate)cavitand **21** and self-assembly of **21** in the presence of Zn^{2+} or Cu^{2+} ions.

To ensure the integrity of the assemblies in solution, stable connections between the building blocks of the cages are required. Figure 8 shows an example of an aggregate that has been characterized in the solid state by X-ray diffraction analysis, while no evidence for intact coordination cages in solution were obtained.³⁷ The assembly **25** contains six tetra(carboxyl)cavitands **24** that are stitched together by Zn^{2+} ions coordinated to the carboxylate groups. In the solid state, one-dimensional coordination polymers of the coordination cages **25** are formed by aggregation through linear μ -hydroxy- or μ -oxo-linkages. Attempts to provide evidence for discrete hexameric species in solution by ESI-MS or NMR spectroscopy have not been successful. The insufficient stability of the aggregates can be attributed to the weak connection of the cavitands *via* the carboxylate groups at the *upper rim* coordinated to zinc ions.

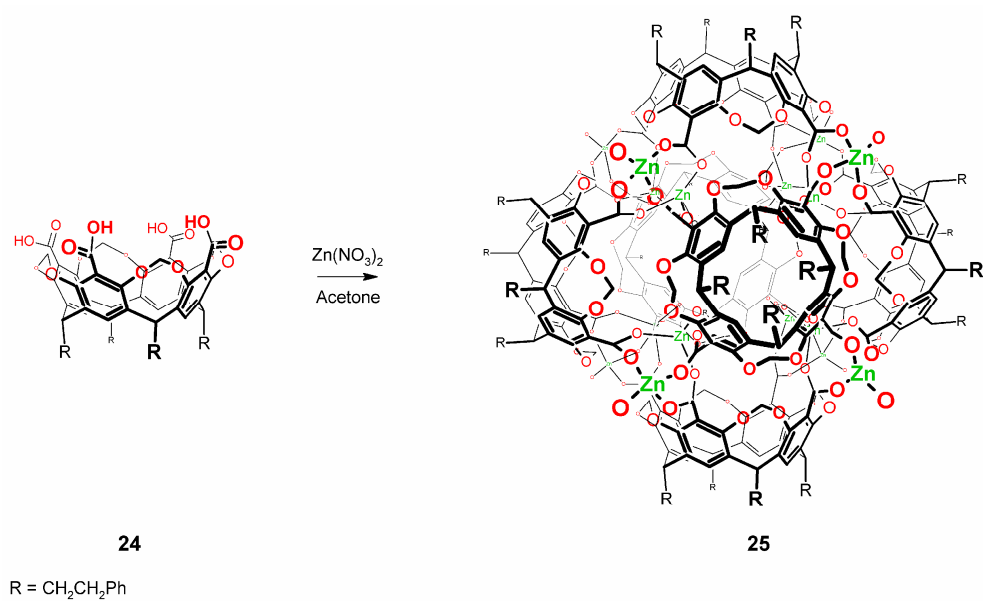


Figure 8: Formation of the hexameric assembly **25** contained in the coordination polymer (which is not shown for clarity).

2.4 Terpyridines as Building Blocks for Coordination Cages

2,2':6',2''-Terpyridine is a common metal-binding domain, which has been increasingly used as a supramolecular motif in the past 20 years.^{38,39} Due to the *meridional* orientation of this terdentate ligand, its *bis*-complexes with metal centers preferring an octahedral coordination geometry can be used as linear connecting units (Figure 9). As the metal center determines the dynamic properties of the complexes, highly directional linkages that are kinetically inert ($M = \text{Co}^{3+}$, Cr^{3+} , Fe^{2+} , Ru^{2+}) or kinetically labile ($M = \text{Zn}^{2+}$, Cd^{2+}) can be realized.

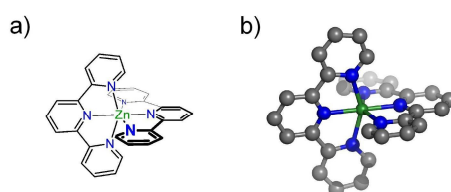


Figure 9: (a) Structure of 2,2':6',2''-terpyridine and $[\text{Zn}(\text{tpy})_2]^{2+}$. (b) Molecular structure of $[\text{Zn}(\text{tpy})_2]^{2+}$ as determined by X-ray diffraction analysis.⁴⁰

Besides metallocycles, metallodendrimers and metallosupramolecular polymers,³⁹ few examples of hollow supramolecular architectures have been obtained from polytopic ligands containing terpyridine units. LEHN *et al.* used heteroaromatic ligands with terpyridine type coordination sites to obtain cylindrical self-assembled architectures (Figure 10).⁴¹ For the synthesis of the cage **28**, tris-2,4,6-(2-pyrimidyl)-1,3,5-triazine (**26**) was mixed with lead triflate in acetonitrile. After 2 h at room temperature, ligand **27** was added and the solution stirred overnight at room temperature. In the assembly **28**, the lead ions are coordinated by six nitrogens of the chelating heterocycles and two triflate ions (which are omitted in Figure 10 for clarity). The highly symmetrical structure is reflected in the ¹H-NMR spectrum, which contains only two sets of signals for the ligands **26** and **27**.

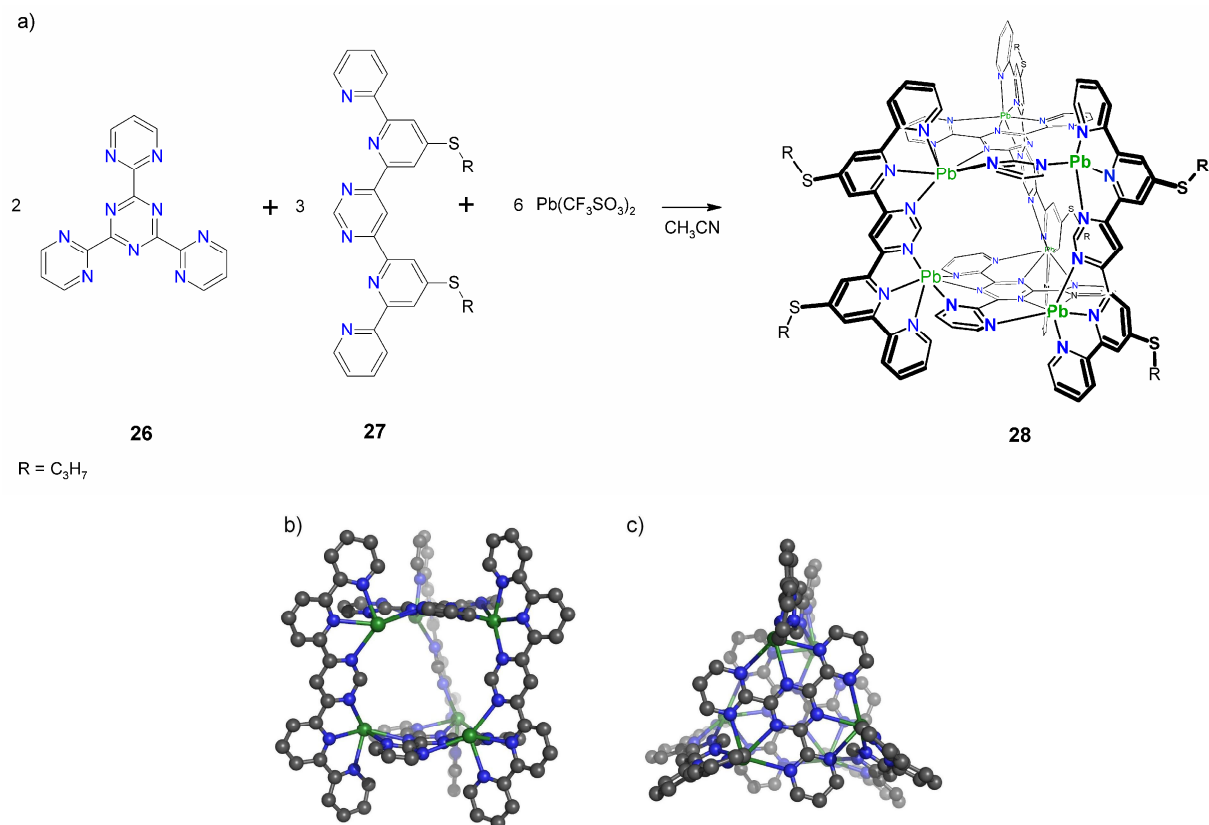


Figure 10: (a) Formation of the cylindrical cage **28** by self-assembly. (b), (c) Structure of **28** as determined by X-ray diffraction analysis ((b) side view, (c) top view, substituents and coordinated triflate ions omitted).

The extended scaffolding ligand **30** is also suited to yield a cylindrical coordination cage (Figure 11). The assembly **31** was characterized by ESI-MS and NMR spectroscopy. The ^1H -NMR spectrum of the highly symmetrical aggregate shows one set of signals for the ligands **30** and two sets of signals for the ligands **29**, which were attributed to the cap ligands at the top and the bottom of the assembly and the ligand in the interior.

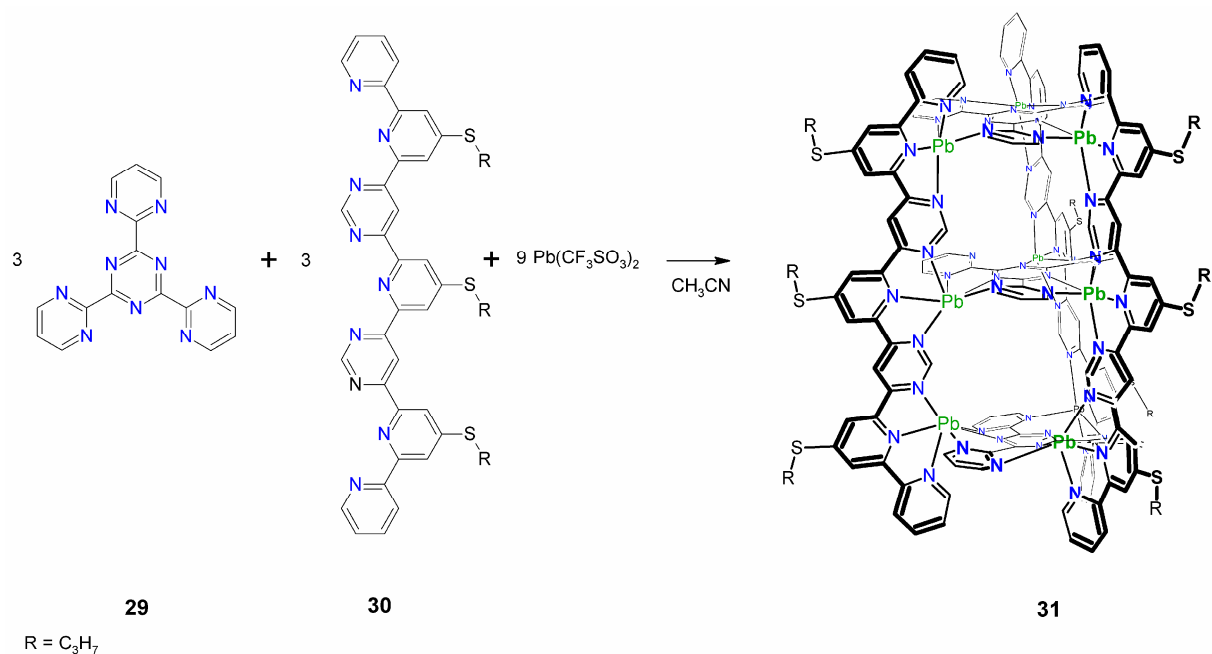


Figure 11: Association of **29** and **30** to the cylindrical cage **31**.

SCHMITTEL *et al.* prepared nanoprisms by heteroleptic aggregation of terpyridine and phenanthroline containing ligands in the presence of Zn^{2+} ions (Figure 12).⁴² In the ditopic ligand **33**, the phenanthroline moieties are substituted by bulky aryl groups. These substituents prevent the formation of homoleptic $[Zn(\text{phenanthroline})_2]^{2+}$ complexes. Thus, heteroleptic zinc complexes can be selectively prepared by coordination of the bis-phenanthroline ligand **32** to Zn^{2+} and subsequent addition of the tris-terpyridine ligand **33** (HETTAP-approach, HETeroleptic Terpyridine And Phenanthroline aggregation).⁴³ When the tritopic terpyridine ligand **33** is added to a solution of the ditopic phenanthroline ligand **32** and Zn^{2+} , self-assembly yields discrete nanoprisms **34**. In agreement with the proposed structure, the $^1\text{H-NMR}$ spectrum showed only one set of signals for the (panneling) ligand **32** and one set of signals for the (scaffolding) ligand **33** that spans the edges of the prism.

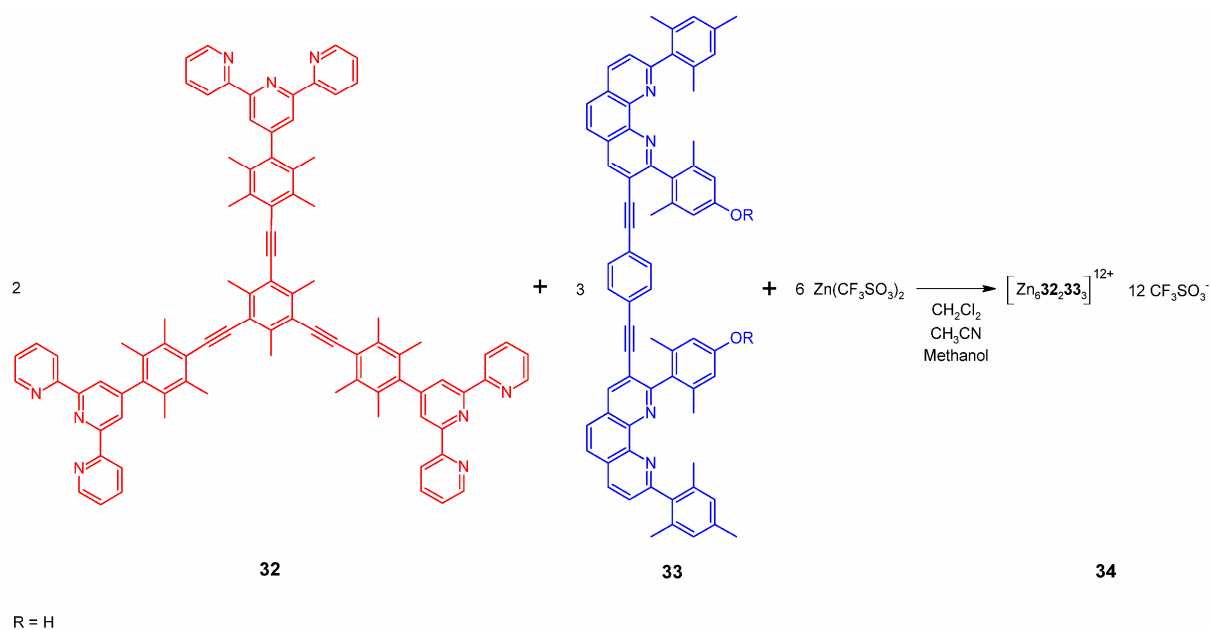


Figure 12: Formation of the nanoprism **34** by heteroleptic aggregation.

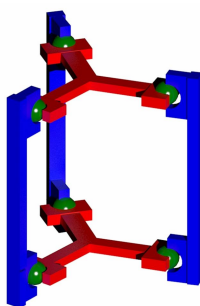


Figure 13: Schematic representation of the proposed structure.

The sensitivity of the self-assembly process towards the ligand design is reflected in the association of the ligands **35** and **36** in the presence of copper ions (Figure 14).⁴⁴ In contrast to **32** and **33**, ditopic terpyridyl ligands and tritopic phenanthroline ligands were used. Reaction of **36** with Cu^{1+} ions and subsequent addition of the bis-terpyridyl ligand **35** yielded a product mixture with the expected metallocsupramolecular cage as a minor component. A templating effect was successfully used to realize quantitative formation of the prismatic structure: In the presence of appropriate guest molecules as C_{60} or a trispyridine (TP), the self-assembly of the cages proceeded smoothly.

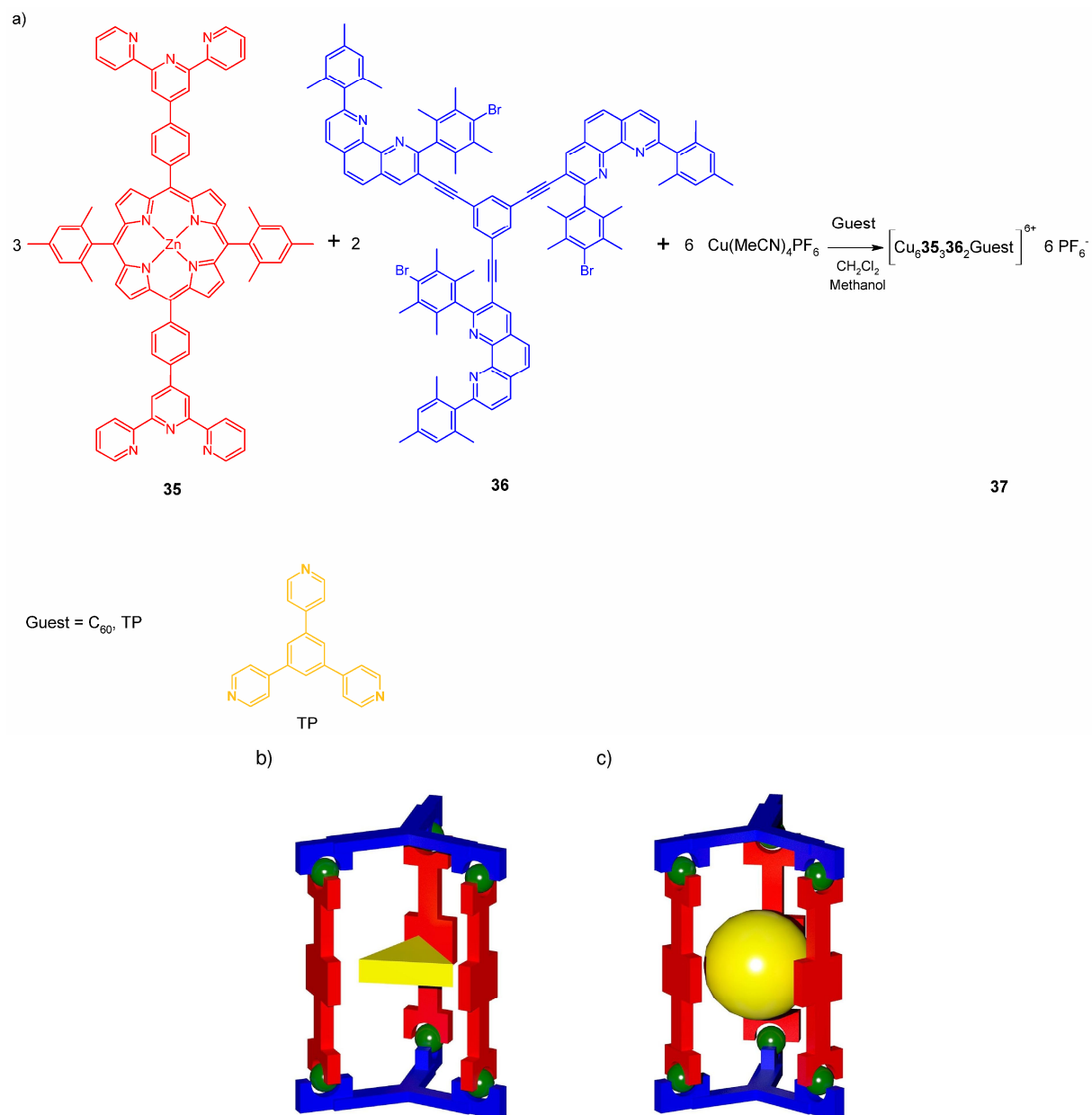


Figure 14: (a) Self-assembly of filled nanoprisms **37**. (b) and (c) Schematic representation of the proposed structures.

2.5 Objective

For the study of processes in confined spaces and effects of compartmentalization, the synthesis of large supramolecular capsules is of considerable interest. Cavitands and calix[n]arenes are valuable building blocks for such hydrogen bonded assemblies and coordination cages due to their shape and the wide range of functional groups that can be introduced at four positions of the cyclophanes. Though several supramolecular capsules have been obtained from the much more flexible calix[4]arenes, the increased preorganization of the cavitand basis can provide enhanced control of metal-directed self-assembly of the tetratopic ligands. To prevent intramolecular complexation of metal ions and constrain the potential geometries of the self-assembled structures, rigid attachment of the metal coordinating groups is of major importance.

Transition metal complexes of 2,2':6',2''-terpyridine are highly directional connecting units ideally suited to bridge the bowl-shaped building blocks. The chelating terpyridine group coordinates *via* three nitrogen atoms of the pyridyl rings and ensures a stable connection to various metal ions in different oxidation states. Because of the space requirements of the heteroaromatic rings of this metal-coordinating group, the aggregation of the building blocks to large assemblies is likely to be preferred compared towards dimeric structures, which are frequently obtained from sterically unconstrained cavitands and for calix[4]arenes.⁸

With the synthesis of large supramolecular coordination cages based on cavitands and calix[n]arenes new hosts for the simultaneous encapsulation of several guest molecules will be provided. The application of bis-terpyridine complexes as bridging units in the synthesis of coordination cages may open the way to large, stable and functional supramolecular assemblies.

2.6 Results:

Synthesis of a Large Metallosupramolecular Cage

For the synthesis of a cavitand functionalized with terpyridyl groups *via* rigid linkages, transition metal catalyzed cross-coupling reactions are especially well suited. Starting with the boronic acid ester **39**,⁴⁵ attachment of the terpyridyl groups to the cavitand was realized by Suzuki-Miyaura reaction with the tetraiodocavitand **38** (Figure 15).

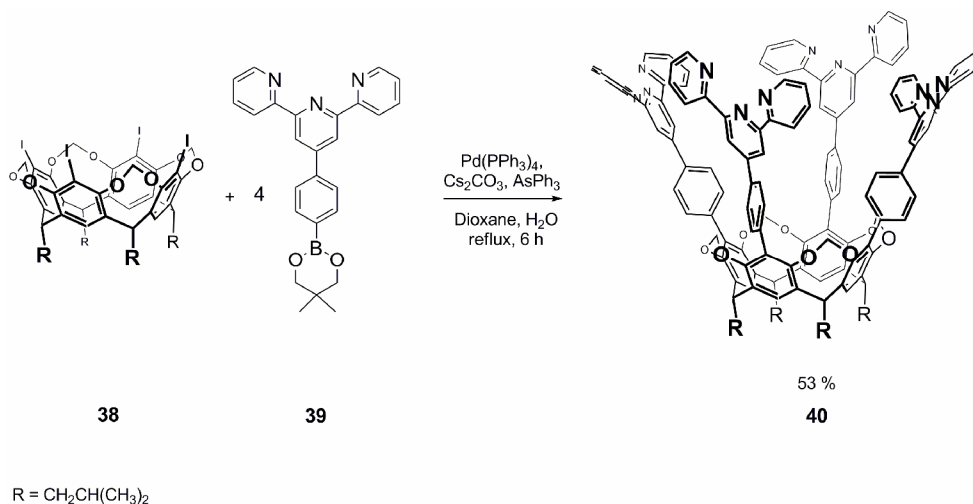


Figure 15: Preparation of a tetra-(4-(2,2':6',2''-terpyridyl)-phenyl)-cavitand **40**.

Initial attempts to prepare a self-assembled spheroidal cage using zinc triflate yielded a colorless solid which was insoluble in organic solvents.

To increase the solubility of the aggregates formed, the large lipophilic TFPB anions (TFPB = tetrakis-(3,5-bis-(trifluoromethyl)-phenyl)-borate) were used instead of the triflate anions.⁴⁶ The zinc salt $[\text{Zn}(\text{NCMe})_6][\text{TFPB}]_2$ **41** was obtained by reaction of zinc bromide with $\text{Ag}(\text{TFBP})$ in acetonitrile under exclusion of light. Addition of tetrahydrofuran- d_8 to a mixture of the cavitand **40** and the zinc salt **41** gave the coordination cage **42** after keeping the reaction mixture at 60 °C for 1 h.

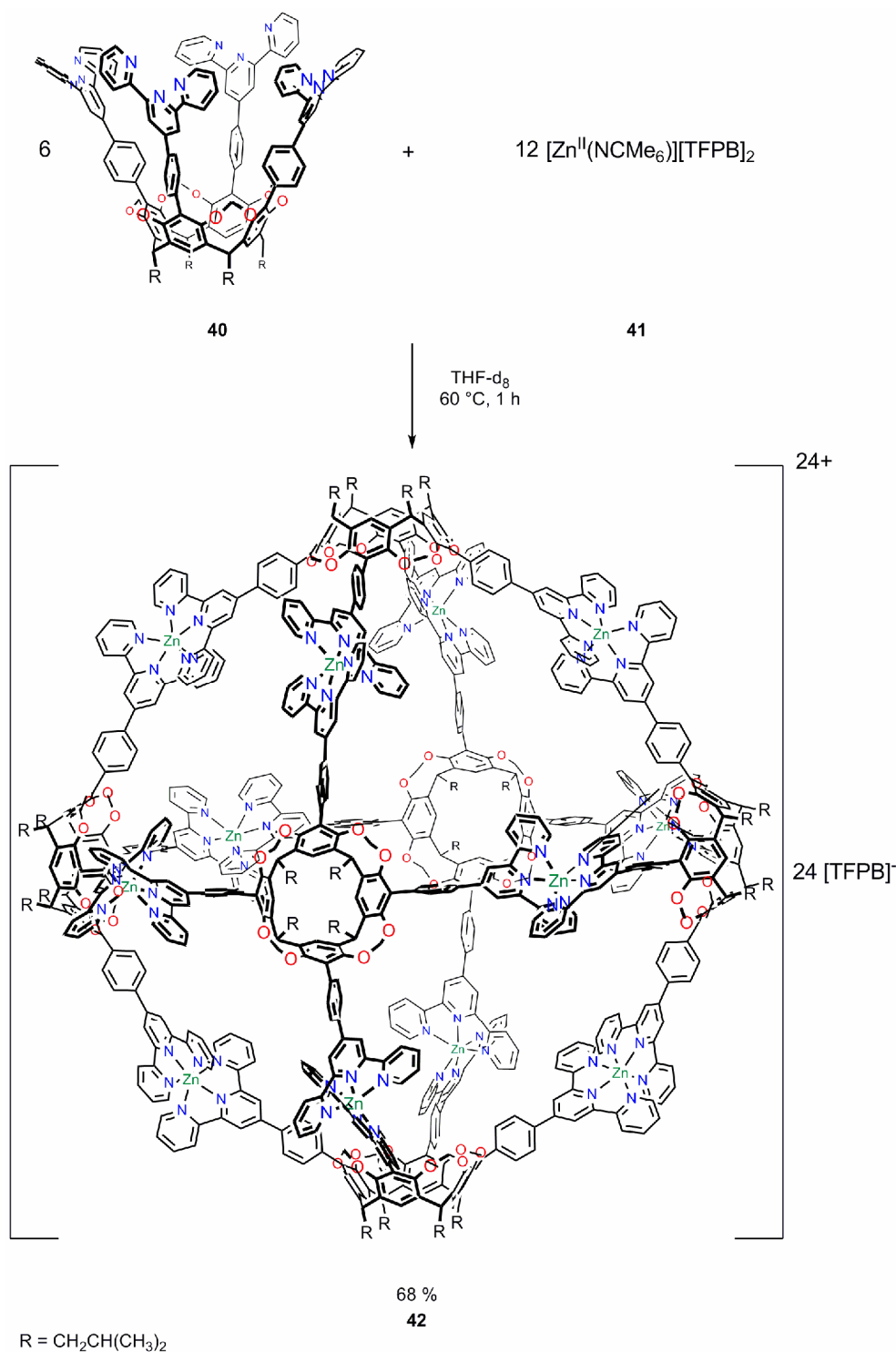


Figure 16: Synthesis of the hexameric assembly 42.

The product, which was readily soluble in organic solvents including acetone, tetrahydrofuran and methylene chloride, was characterized by ESI-MS, 1H - and ^{13}C -NMR spectroscopy, diffusion NMR spectroscopy, SAXS measurements and elementary analysis. In the ESI-MS, multiply charged ions $[42-n TFPB]^{n+}$ with $n = 7 - 11$ containing the intact coordination cage were observed exclusively (Figure 17). The isotope pattern prove the charge states of the ions and confirm the hexameric nature of the aggregate.

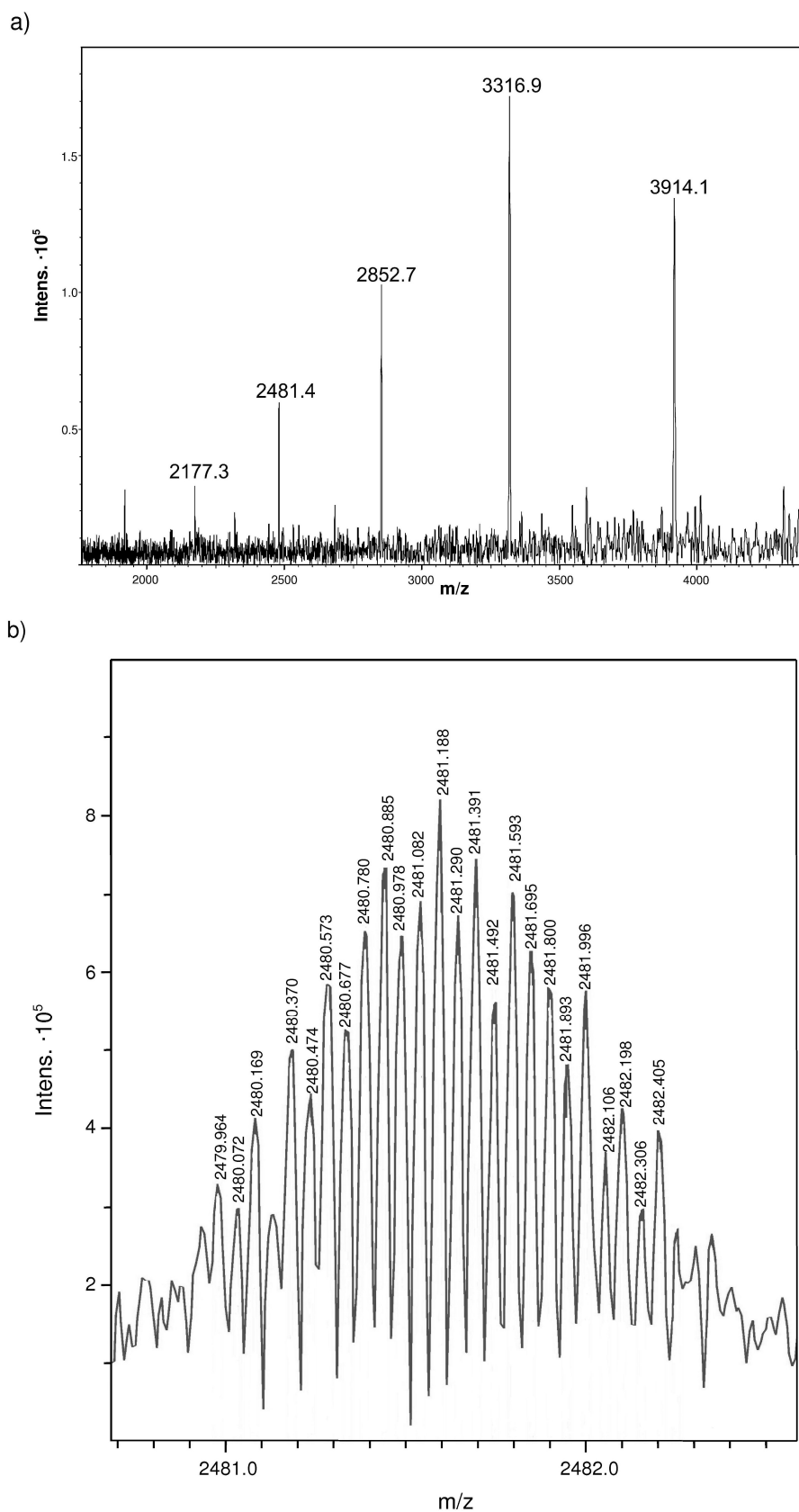


Figure 17: (a) ESI-MS of **42**. (b) Isotopically resolved pattern observed for $[\mathbf{42}-10\text{TFPB}]^{10+}$.

The ^1H - and ^{13}C -NMR spectra indicate a highly symmetrical structure of **42** (Figure 18). For all six cavitands in the assembly, only one set of signals is observed. Furthermore, even for the 2,2':6',2''-(terpyridyl)phenyl groups only five different resonances are detected, which can be explained with a rotation of the terpyridyl groups resulting in a fast exchange at the NMR time scale at room temperature. The characteristic shift of the signals of the hydrogen atoms in *meta*- and *ortho*-position to the nitrogen atoms compared to the resonances of free cavitand **40** signifies the coordination of the Zn^{2+} ions by the terpyridyl groups.

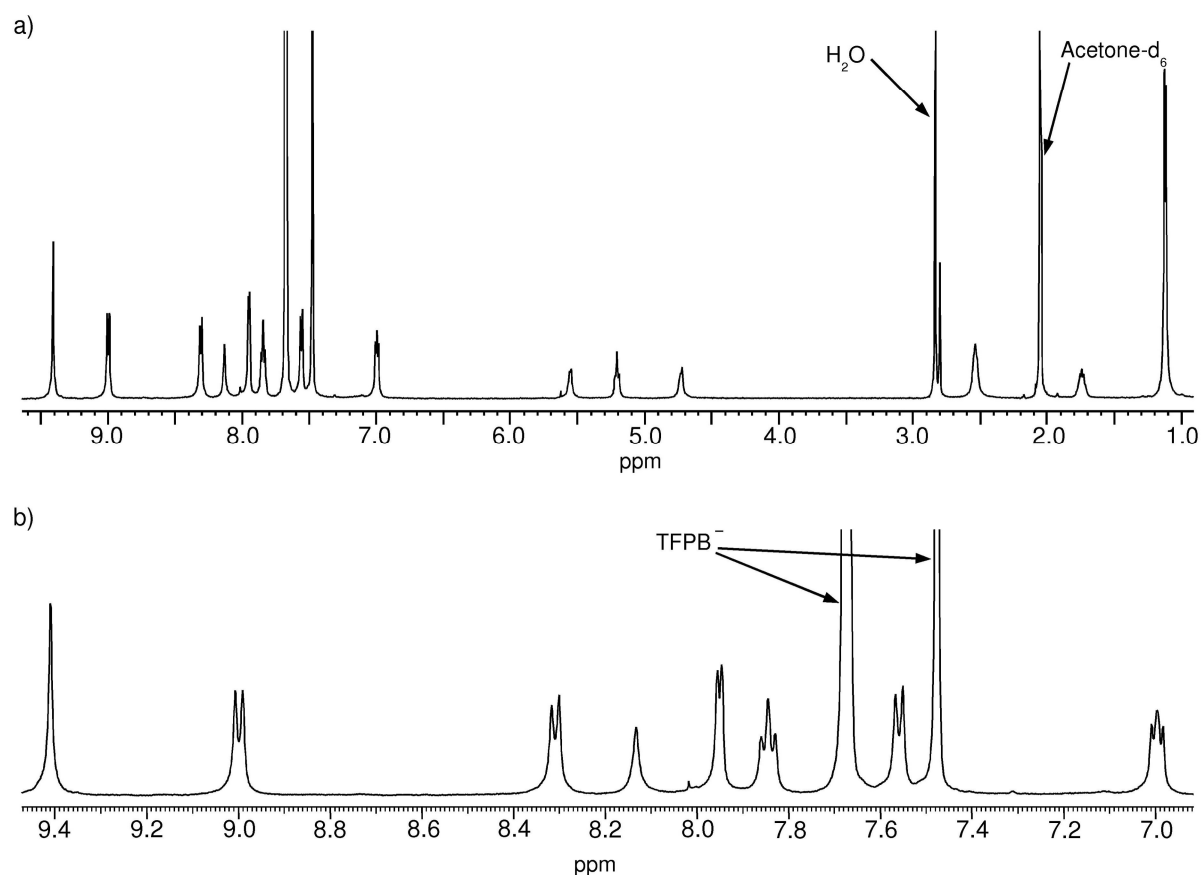


Figure 18: (a) ^1H -NMR spectrum (500 MHz) of **42** in acetone-d_6 . (b) Zoom into the aromatic region.

Diffusion NMR spectroscopy experiments were carried out to determine the diffusion coefficient D of the cavitand **40** and the coordination cage **42**.⁴⁷ While for the free cavitand **40** a diffusion coefficient of $D = (4.91 \pm 0.04) \cdot 10^{-10} \text{ m}^2 \cdot \text{s}^{-1}$ was obtained, a significantly slower diffusion ($D = 2.06 \pm 0.05) \cdot 10^{-10} \text{ m}^2 \cdot \text{s}^{-1}$) was observed for the large assembly **42** in tetrahydrofuran- d_8 at 20 °C. Assuming a nearly spheroidal form, the diameter of **42** was estimated to be 4 nm.

SAXS (Small Angle X-ray Scattering) measurements performed by Markus Tonigold in the group of Prof. Dirk Volkmer at Ulm University provided further insight into the structure of the assembly in solution.⁴⁸ Using the GNOM/DAMMIN software packages, the SAXS data were used to reconstruct a low resolution three-dimensional particle shape (yellow semitransparent spheres in Figure 19).⁴⁹ The obtained radius of gyration as well as the reconstructed shape is in very good agreement with the expected dimensions of the coordination cage **42** (Figure 20).

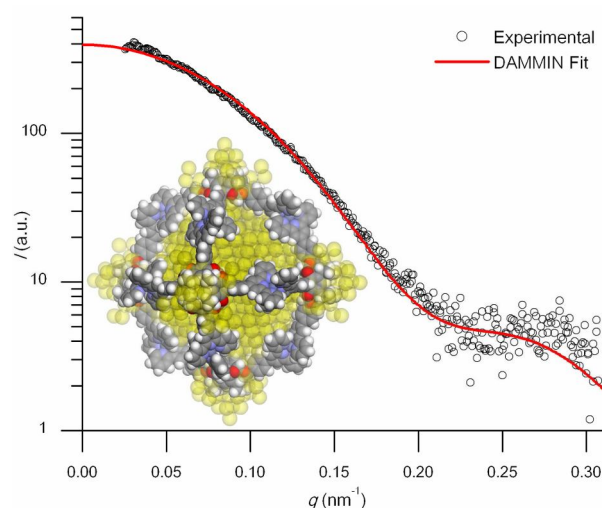


Figure 19: Main plot: SAXS intensity (I) vs. momentum transfer for a solution of **42** in acetonitrile ($5.1 \text{ g}\cdot\text{L}^{-1}$).

The symbols and the solid line correspond to the experimental data points and the numerical fit using GNOM/DAMMIN simulated annealing, constraining the symmetry to the point group $P432$ ($\chi = 1.397$). Inset: reconstructed low-resolution particle shape for **42** obtained by the GNOM/DAMMIN fit (semitransparent spheres) superimposed to the PM3 stationary point (space-filling model, *iso*-butyl groups substituted by methyl groups).

Attempts to grow single crystals suitable for X-ray diffraction analysis of **42** failed. Therefore, the structure of the assembly **42** (*iso*-butyl groups substituted by methyl groups) was optimized by Dr. Ralf Brodbeck under the constraint of O symmetry using the semiempirical PM3 method (Figure 20).⁵⁰ In the modeled structure, the cavitands lie at the apices of an octahedron. The edges of the platonic solid are defined by the zinc ions coordinated to the terpyridyl groups. While the largest distance of the zinc ions at opposite edges is approximately 3.9 nm, the largest distance between the methyl groups are 4.6 nm. According to the calculations, openings with a minimal diameter of 0.77 nm exist between adjacent bis-terpyridyl zinc complexes. Based on the modeled structure, the size of the inner cavity was evaluated with the program CARVER.⁵¹ The largest sphere that fits into the capsule has a diameter of approximately 3 nm, which corresponds to a volume of about 14 nm^3 . A force field calculation of the gas phase energy minimized structure demonstrates that up to seven TFPB anions could be encapsulated, illustrating the dimensions of the inner cavity.

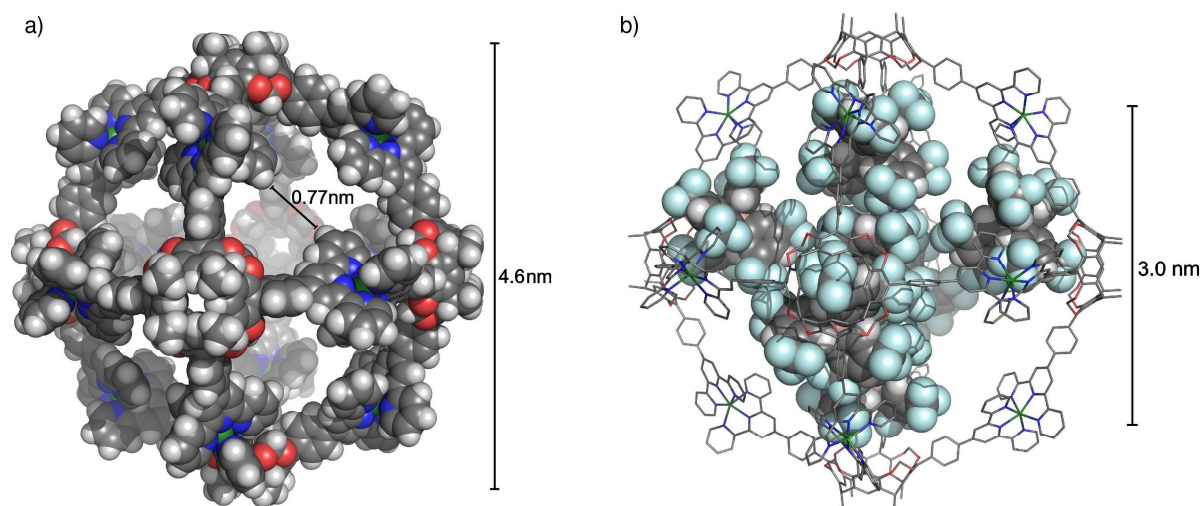


Figure 20: (a) Space-filling representation of the *O*-symmetric stationary point of the methyl derivative of **42** on the PM3 hypersurface. (b) Representation of the energy minimized structure of the methyl derivative **42** containing seven TFPB anions obtained from a force field calculation.

In cooperation with the group of Prof. Dr. Dirk Volkmer (Ulm University), the synthetic procedure established for the preparation of the tetra-(4-(2,2':6',2''-terpyridyl)-phenyl)-cavitand **40** was adapted for the synthesis of terpyridyl-substituted calix[*n*]arenes.⁵² The tetra-(4-(2,2':6',2''-terpyridyl)-phenyl)calix[4]arenes **45 a** and **45 b** and the penta-(4-(2,2':6',2''-terpyridyl)-phenyl)calix[4]arene **46** can be prepared from the boronic acid ester **39** and tetrabromocalix[4]arene **43 a** or **43 b** and pentabromocalix[5]arene **44**, respectively (Figure 21).

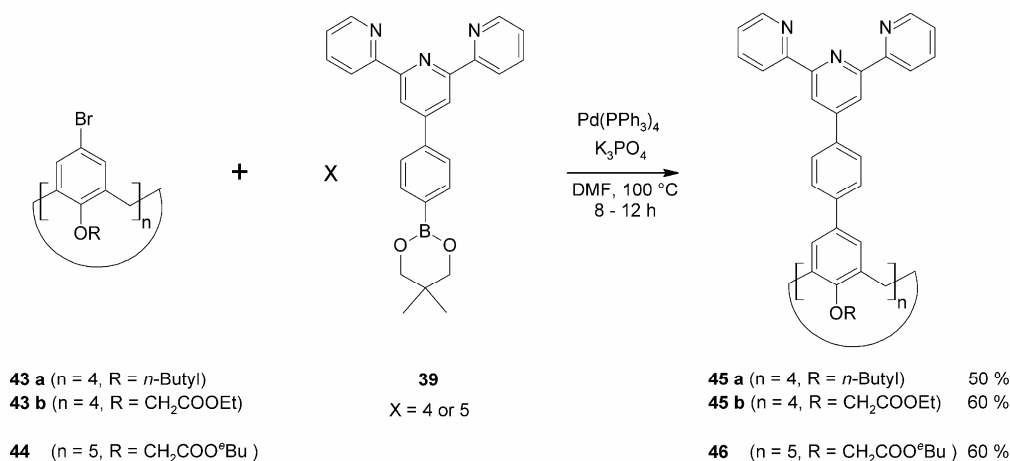


Figure 21: Synthesis of terpyridyl-substituted calix[*n*]arenes.

The flexibility of the calix[4]arene basis is reflected in the molecular structure of **45a** as determined by X-ray diffraction analysis (Figure 22). The calix[4]arene adopts a *flattened cone* conformation with intramolecular π -stacking of two terpyridyl units. While the hexameric coordination cage **42** has been obtained from the rigid terpyridine-substituted cavitand **40**, the lower degree of preorganization of the calix[n]arenes leads to a significantly different self-assembly in the presence of Zn^{2+} ions with a variety of species formed as determined by ESI-MS and $^1\text{H-NMR}$ spectroscopy.

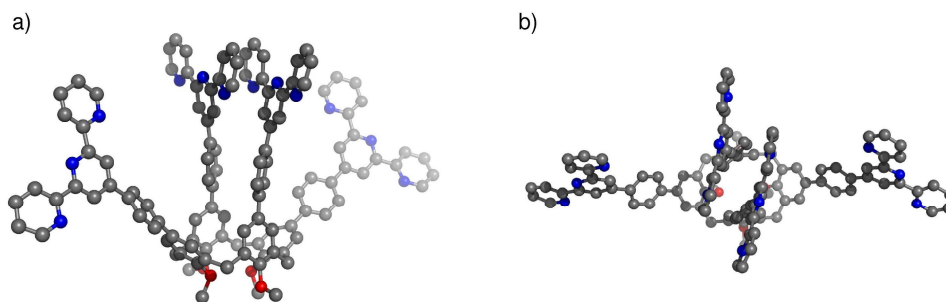


Figure 22: Structure of **45a** as determined by X-ray diffraction analysis.

In conclusion, a large metallocupramolecular capsule **42** based on a terpyridyl-substituted cavitand has successfully been synthesized. The low flexibility of the methylene-bridged cavitand units and the rigid attachment of the terpyridyl groups to the cavitand basis yields the highly preorganized tetratopic ligand **40**. The relative orientation of the metal coordinating sites is suited for the self-assembly of **40** in the presence of zinc ions to the stable, highly symmetrical coordination cage **42**. To prevent irreversible formation of insoluble precipitates during self-assembly, the use of lipophilic anions as tetrakis-(3,5-bis-(trifluoromethyl)-phenyl)-borate (TFPB) is essential. The structure of the hexameric assembly has been modeled using semiempirical PM3 method. According to the calculated structure and in agreement with experimental data from diffusion NMR and SAXS measurements, the diameter is approximately 4.5 nm. The size of the inner cavity of the aggregate is characterized by the diameter ($d = 3$ nm) of the largest sphere that fits into the capsule and is large enough to encapsulate several bulky molecules. Therefore, this coordination cage is an example for a large molecular flask, which can be used for the stabilization of reactive species or as nanoscale reaction chambers.⁵³ To realize such advanced applications, the encapsulation of guest molecules in the cage **42** will be investigated in further studies.

The synthetic route to the cavitand **40** can with minor changes be applied to synthesize terpyridyl-substituted calix[4]arenes **45 a** and **45 b** and the calix[5]arene **46**. Due to the higher flexibility of the cyclophane basis, the self-assembly behaviour of these ligands is significantly different, yielding product mixtures upon addition of zinc ions. Besides templating effects of appropriate guest molecules, the introduction of substituents at the *narrow rim* of the calix[n]arene basis might be a possibility to rigidify the ligand and gain enhanced control over the self-assembly process.

3 Dynamics and Stability of Hydrogen-bonded Supramolecular Capsules

3.1 Self-Assembly Dynamics of Supramolecular Capsules

While several hydrogen-bonded supramolecular capsules have been synthesized, less is known about the self-assembly dynamics of these systems in solution. The kinetics of the hydrogen-bonded capsules based on calix[4]arenes substituted with urea functions at the *wider rim* (see section 2.2) has been analyzed by NMR spectroscopy and FRET measurements (Figure 23 and 24). To evaluate the exchange of capsule subunits by NMR, a tetra(urea)calix[4]arene **47** with two methyl groups and two pentyl groups at the *narrow rim* has been synthesized.⁵⁴ By introducing the methyl and pentyl substituents, the symmetry of the associate is reduced. Therefore, the two calix[4]arenes in the dimer are nonequivalent and separate signals are observed for the building blocks in the $^1\text{H-NMR}$ spectrum. This is essential for the analysis of the dynamic process by NMR spectroscopy. Based on the NOE intensities between signals of hydrogens of the different calix[4]arenes in the dimer, an exchange rate of $k = 0.26 \text{ s}^{-1}$ has been determined in benzene- d_6 .

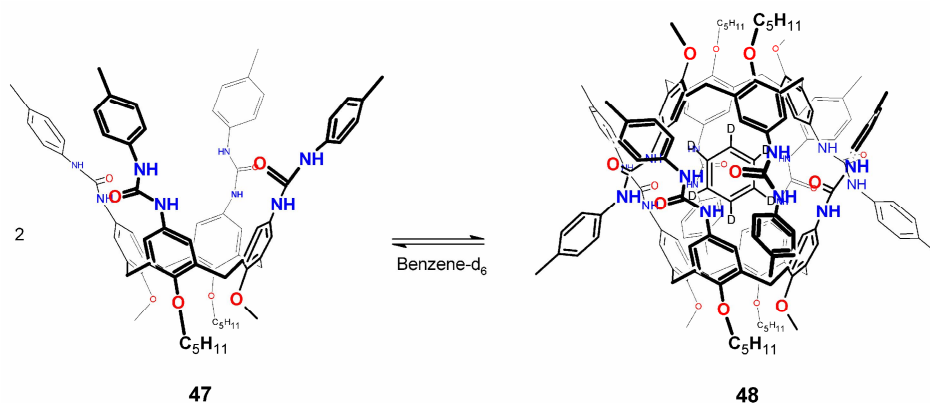


Figure 23: Self-association of the tetra(urea)calix[4]arenes **47** with methyl and pentyl groups at the *narrow rim*.

A detailed analysis of the association of homo- and heterodimeric capsules of similar tetra(urea)calix[4]arenes has been carried out using FRET measurements in benzene (Figure 24).⁵⁵ For this experiment, the building blocks were labeled at the *narrow rim* with fluorophores. Formation of the dimer **51** was indicated by acceptor emission due to energy transfer between donor (D) and acceptor (A), which was not detected for free labeled calix[4]arenes. While fast association was observed for tetra(urea)calix[4]arenes ($k_{\text{ass}} = 10^3 - 10^4 \text{ s}^{-1}$), the dissociation was much slower ($k_{\text{diss}} = 10^{-3} - 10^{-6} \text{ s}^{-1}$). The discrepancy in the dissociation rate constants obtained from the NMR and the FRET studies were explained with differences in the structure of the building blocks and a concentration dependence of the rate constants.

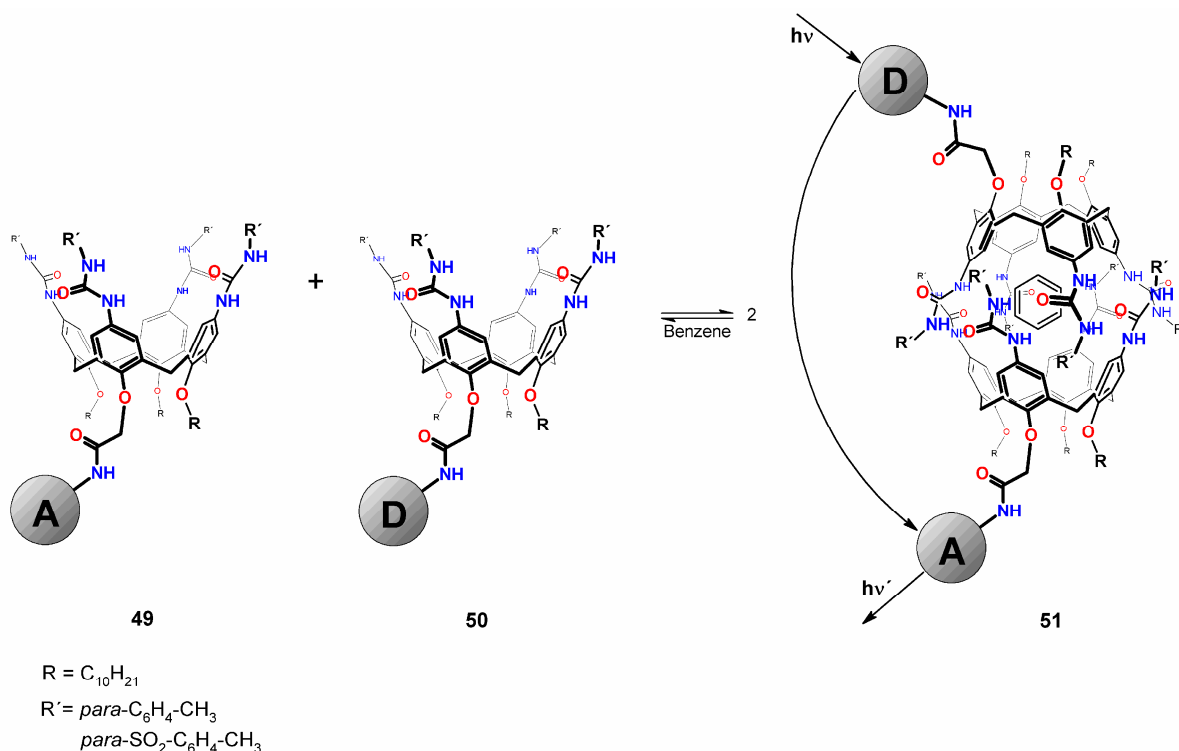


Figure 24: Setup of the FRET experiment: Exchange of donor (D) and acceptor (A) labeled capsule subunits results can be monitored by acceptor emission.

A second type of dimeric capsules analyzed by FRET measurements is based on cavitands stitched together by eight hydrogen bonds (Figure 25).⁵⁶ Attachment of fluorescent dyes to the monomers allowed the observation of dynamic processes. Upon mixing solutions of the capsules **52** and **53** composed of acceptor- (A) and donor- (D) labeled building blocks, acceptor emission was observed due to exchange of capsule subunits. While assembly of the capsule is known to occur very rapidly, the rate constant for exchange of the subunits was determined to be $k = 1.9 \cdot 10^{-3} \text{ s}^{-1}$ in toluene.

Further studies were carried out in mesitylene (which is an ill-fitting guest for the capsule) to evaluate the influence of different encapsulated guest molecules on the stability of the system. In the presence of *n*-alkanes, 4,4'-substituted biphenyls or 4,4'-disubstituted benzanilides, the exchange rate was strongly reduced to up to $k = 2.7 \cdot 10^{-6} \text{ s}^{-1}$ depending on the size of the guest molecule. These results clearly show that capsule association is highly adjustable and host-guest interactions have an important influence on the bonding of the supramolecular complex.

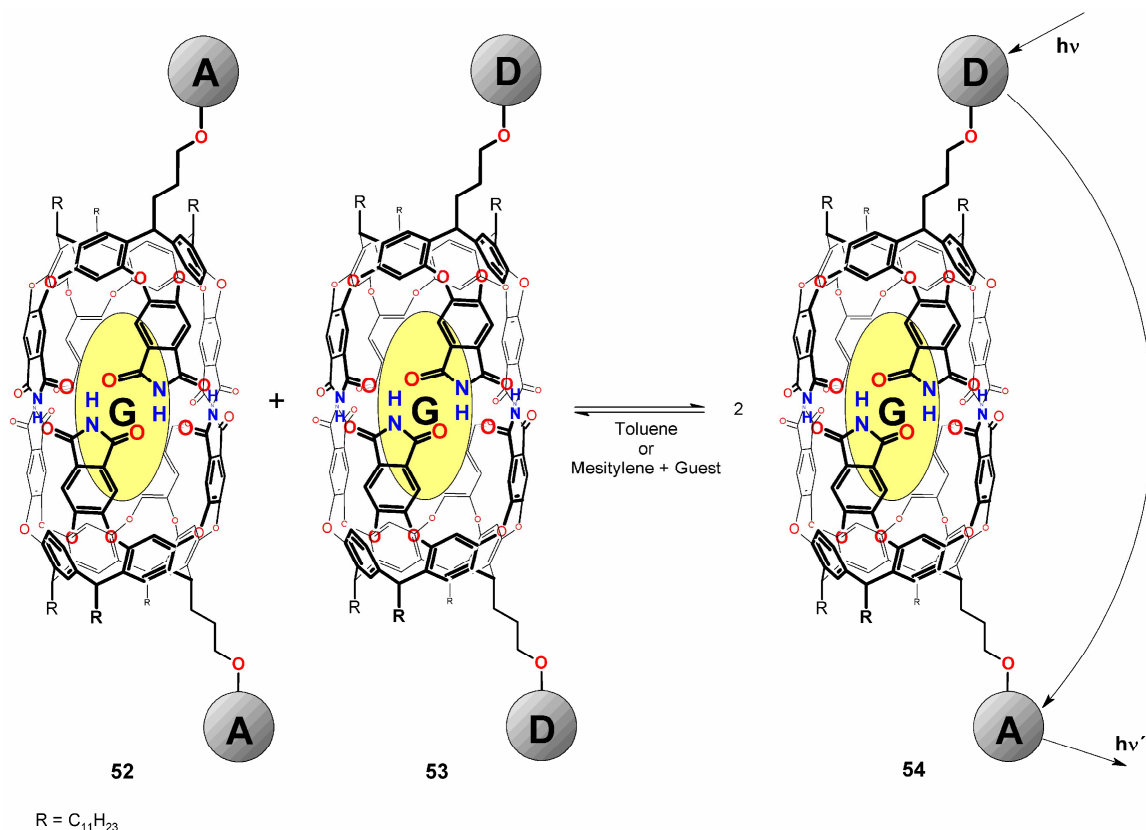


Figure 25: Setup of the FRET experiment to determine the exchange rate of the subunits of a dimeric cavitated capsule. The encapsulated guest (G) has a strong influence on the stability of the capsule.

3.2 Atomic Force Single-Molecule Force Spectroscopy (AFM-SMFS)

The atomic force microscope (AFM) is a versatile tool for various imaging and manipulation applications at the (sub-)nm scale.^{15,57} The basic setup consists of a small force sensor (cantilever) and a piezo scan tube on which the sample is placed to precisely control the relative position of the cantilever and the sample in horizontal and vertical direction (Figure 26). The interaction between the sharp tip of the cantilever (tip radius ≈ 10 nm) and the substrate is transduced to minimal deflections of the force sensor that can be measured by the displacement of a laser beam which is reflected from the back of the sensor and detected by a quadrant detector.⁵⁸ The feedback loop electronics allows an exact control of the forces acting between tip and sample, which is the precondition for topographic scans. In addition to the imaging, nano-scale objects can be precisely manipulated with the cantilever tip by applying very low forces in the range of piconewtons ($1 \text{ pN} = 10^{-12} \text{ N}$).

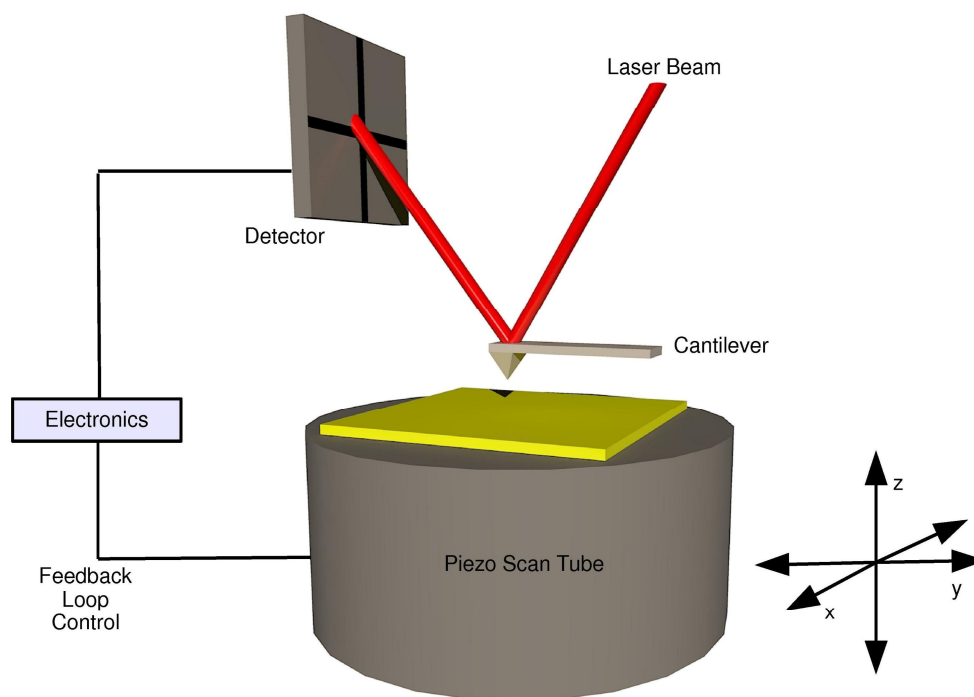


Figure 26: Setup of an atomic force microscope (AFM).

To probe the interactions between a ligand and a receptor in an AFM-SMFS experiment, the cantilever surface is functionalized with a ligand *via* a flexible PEG linker and is approached to a substrate with the immobilized receptor (Figure 27).^{12,13,59} While the cantilever tip is in contact with the substrate, the ligand can access the receptor cavity due to the flexible PEG linker and the complex is formed. When the cantilever is withdrawn, the linker molecule is uncoiled and stretched, resulting in a force acting on the ligand-receptor bond. Finally, the molecular complex dissociates under the externally applied force.

The deflection of the force sensor during this experiment is detected and allows the evaluation of the forces required for the rupture of the ligand-receptor bond. In Figure 27 a, a typical force-distance curve is shown. While first uncoiling of the PEG linker proceeds without significant deflection of the cantilever, stretching of the chain-like polymer results in a force load acting on the complex reflected in a non-linear force profile. When the ligand-receptor bond dissociates, the cantilever snaps back to the zero-force position and a distinct force jump (rupture force) is detected. Due to the stochastic nature of the thermally activated dissociation process, this approach-retract-cycles have to be repeated many times (typically 500) and the measured dissociation forces are plotted in a histogram. The distribution can be fitted with a Gaussian distribution to yield the most probable dissociation force (f^*) at a given loading rate.

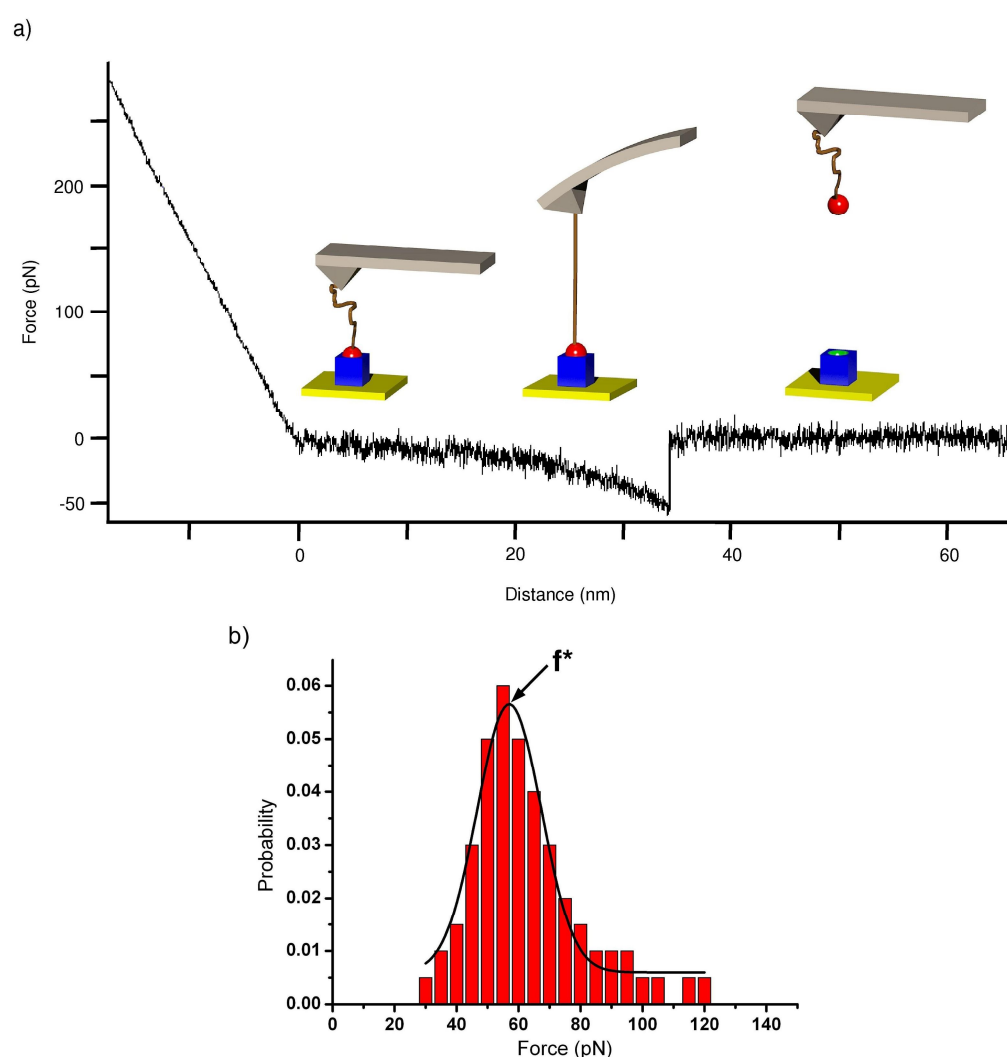


Figure 27: (a) Scheme of the single-molecule force spectroscopy experiment and typical AFM force curve. (b) Histogram of the single-molecule dissociation forces with Gaussian fit to the distribution and the most probable dissociation force f^* .

In this study, all force spectroscopy experiments were performed using a commercial instrument (Multimode AFM with a Nanoscope IIIa controller, Veeco Instruments, Santa Barbara, CA, USA) (Figure 28). The acquisition of the cantilever deflection signal and the vertical movement of the piezo electric element was externally controlled *via* a home-built control electronics based on Labview (National Instruments, Austin, USA). The cantilevers with typical spring constants ranging from 17 to 22 pN/nm (MSCT, Lever C, nominal tip radius \approx 10 nm, Veeco Instruments) were calibrated by the thermal fluctuation method with an absolute uncertainty of 10 %.⁶⁰



Figure 28: Setup used in this study for SMFS experiments.

To realize single-molecule force spectroscopy experiments in *para*-xylene, the fluid cell (Veeco Instruments) was used. The functionalized gold-coated samples (Arrandee, Werther, Germany) were placed in a home-built teflon vessel inert against swelling or deformation in organic solvents (Figure 29).

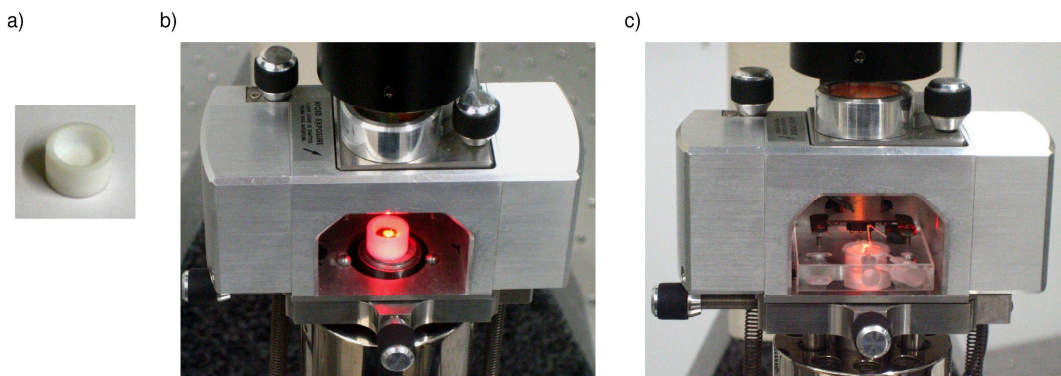
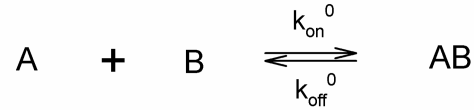


Figure 29: Customized fluid cell setup for measurements in organic solvents. (a) Teflon vessel stable against organic solvents. (b) Sample in teflon vessel mounted on the piezo scan tube. (c) Complete customized setup.

A connection between the mechanical forces acting on the complex and the dissociation rate constant in the absence of an external force has been provided within the BELL-EVANS model.^{16,17} In general, the formation of the complex AB from two components A and B is described by the law of mass action.



k_{on}^0 Rate constant of association

k_{off}^0 Rate constant of dissociation

The equilibrium constant of association (K_{ass}) is given by equation 1 and is under standard conditions related to the standard Gibbs free energy by equation 2.

$$K_{\text{ass}} = \frac{[AB]}{[A] \cdot [B]} = \frac{k_{\text{on}}^0}{k_{\text{off}}^0} \quad \mathbf{1}$$

$$\Delta G^0 = R \cdot T \cdot \ln(K_{\text{ass}}) \quad \mathbf{2}$$

[X] Concentration of component X

T Temperature

R Universal gas constant

According to Arrhenius, the rate constant of dissociation is dependent on the height of the potential barrier (ΔG^\ddagger) (Equation 3).⁶¹

$$k_{\text{off}}^0 \propto e^{-\frac{\Delta G^\ddagger}{k_B \cdot T}} \quad \mathbf{3}$$

k_B Boltzmann constant

In a single-molecule force spectroscopy experiment, a mechanical force is acting on the complex, which leads to a thermally activated dissociation under the externally applied force. Figure 30 schematically shows the influence of the force load on the potential barriers. According to BELL and EVANS, the external force lowers the energy barrier to the unbound state and therefore promotes the dissociation of the complex (Equation 4).

$$\Delta G^\#(f) = \Delta G^\# - f \cdot x_\beta \quad 4$$

x_β molecular reaction length, width of the binding potential
 f force applied on the complex in direction of the reaction coordinate

Therefore, the dissociation rate constant is dependent on the force acting on the complex (Equation 5).

$$k_{\text{off}}(f) = k_{\text{off}}^0 \cdot e^{\frac{f \cdot x_\beta}{k_B \cdot T}} \quad 5$$

While the cantilever is retracted from the substrate in the force spectroscopy experiment, the applied force increases with tip-substrate distance, until finally the bond dissociates. The time-dependent force is given by the product of the cantilever deflection and the effective spring constant c (molecular elasticity), which comprises the spring constant of the cantilever and the elasticity of the polymer linker used to tether the ligand to the cantilever (Equation 6). The product of effective spring constant and retract velocity v_{retract} is the loading rate r .

$$f(t) = c \cdot d = c \cdot v_{\text{retract}} \cdot t = r \cdot t \quad 6$$

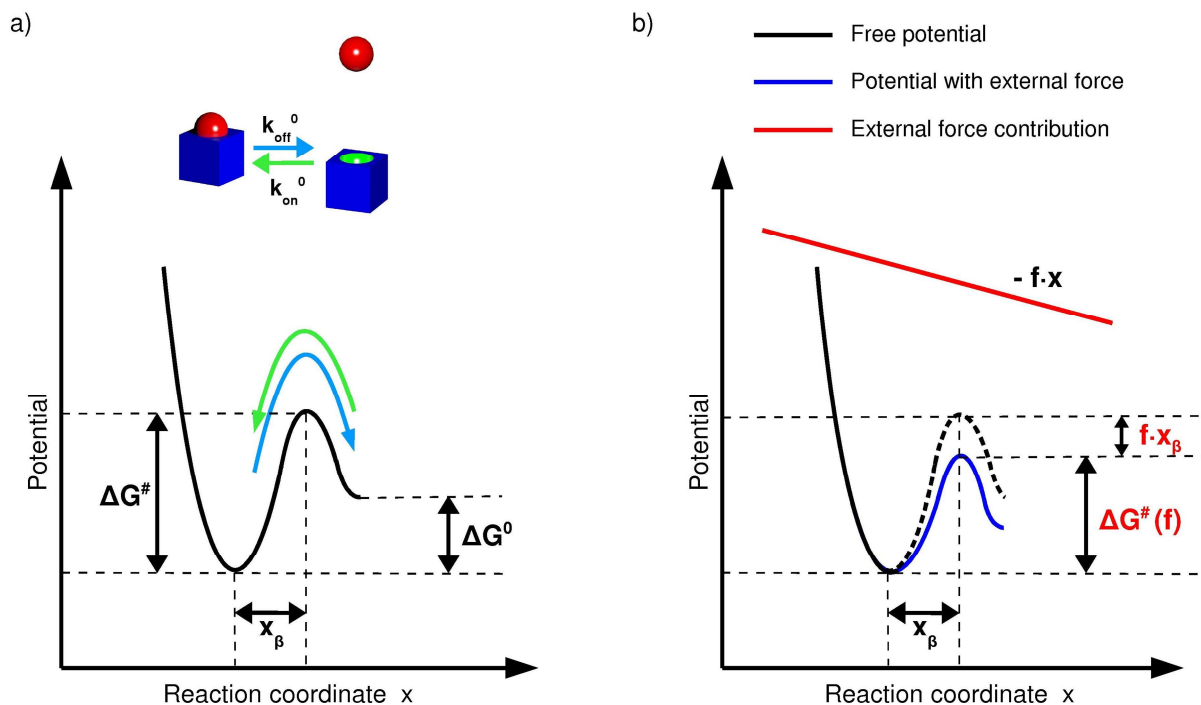


Figure 30: Scheme of the energy barriers between bound and unbound state (a) in the absence or (b) in the presence of an external force acting on the complex.

Based on this model, EVANS and RITCHIE derived an equation that connects the most probable dissociation force determined in single-molecule force spectroscopy experiments with the loading rate r (equation 7).

$$f^* = \frac{k_B \cdot T}{x_\beta} \cdot \ln\left(\frac{x_\beta \cdot r}{k_{\text{off}}^0 \cdot k_B \cdot T}\right) \quad 7$$

According to this equation, the dissociation rate constants in the absence of external force can be determined from single-molecule force spectroscopy experiments carried out at different retract velocities (DFS-SMFS, Dynamic Force Single-Molecule Force Spectroscopy). By plotting the most probable rupture forces f^* vs $\ln(r)$, the molecular reaction length x_β and the dissociation rate constant in the absence of an external force k_{off}^0 can be determined from the slope and the regression of the linear fit to zero force ($f^* = 0$) (Figure 31).

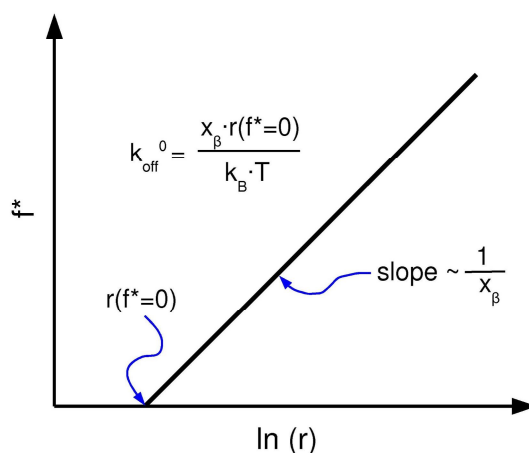


Figure 31: Plotting of the most probable dissociation forces f^* vs $\ln(r)$ and regression allows determination of x_β and k_{off}^0 .

In this standard theory described above, several simplifications are included. For instance it is assumed that the dissociation takes place exactly along the same reaction coordinate in every pulling experiment. In reality the geometry of complex, linker and AFM tip varies with every experiment. Another point is that the total instantaneous force acting on the complex is assumed to depend solely on the total instantaneous extension of all components of the system. This is generally not the case, as the polydispersity of the employed PEG linkers contributes to a spread in the force-extension characteristics. To take the complexity of the experimental parameters into account, an extended model (heterogeneous bond model) has been developed which includes the deviations of the overall system in random variations of the molecular reaction length x_β .⁶² Application of this analysis leads to significantly improved agreement of the experimental data with the theory, as broad distributions of the dissociation forces which are frequently observed in experiments can be explained.

However, in the current study the standard model by EVANS and RITCHIE is applied for data analysis due to the narrow distributions obtained and to achieve comparability with previous work by other groups.

3.3 Single-Molecule Force Spectroscopy of Hydrogen-bonded Supramolecular Systems

Pioneering studies characterizing fundamental supramolecular interactions like hydrogen bonding, coordination bonding, host-guest interaction, hydrophobic interactions and π - π interactions using AFM-SMFS have attracted considerable research interest.^{63–69} Despite the rich information accessible, the technique has rarely been employed to analyze the bonding between synthetic building blocks of complex supramolecular structures.^{63,64,66–70}

VANCSO *et al.* have studied the self-association of 2-ureido-4(1*H*)-pyrimidinone (UPy) **55** and a supramolecular polymer obtained from this quadrupole hydrogen-bonded binding motif (Figure 32).^{63,64} The self-complementary UPy molecules dimerize *via* a donor-donor-acceptor-acceptor (DDAA) array of four hydrogen bonds. The exceptional stability of the association is due to the optimal alignment of the hydrogen bonding sites, that results in predominantly attractive secondary interactions in addition to the hydrogen bonds.⁷¹ For force spectroscopy measurements, UPy was immobilized at gold-coated samples and AFM tips as SAM of poly(ethylene glycol) disulfides or as thiolates. To study the bond strength of the non-covalently bound associate, SMFS experiments were carried out in hexadecane.⁶³ For the UPy dimer, most probable dissociation forces between 148 pN and 269 pN at loading rates of $5.7 \cdot 10^3 \text{ pN} \cdot \text{s}^{-1}$ to $3.4 \cdot 10^5 \text{ pN} \cdot \text{s}^{-1}$ were detected. From the measured data, the average bond lifetime of the UPy-UPy dimer was determined to be $\tau = 5 - 7 \text{ s}$ and the equilibrium constant of association was estimated to be $K = 1 \cdot 10^9 \text{ M}^{-1}$. These results are in good agreement with the values obtained in NMR and fluorescence spectroscopy studies.⁷²

The investigation of a supramolecular polymer based on the UPy-UPy association was realized in measurements in solutions containing the bis-UPy-functionalized poly(ethylene glycol) **57**.⁶⁴ Upon approaching the cantilever-immobilized UPy to the UPy-functionalized gold substrate, association of the surface-bound molecules with free **57** results in the formation of a supramolecular polymer that bridges the gap between the AFM-tip and the substrate. Dissociation of non-covalent interactions in the polymer was observed at tip-substrate distances between 10 nm and 150 nm when the tip was retracted, corresponding to up to 15 monomer units per polymer chain. Because uncooperative bond ruptures can occur throughout the different hydrogen-bonded UPy-UPy dimers in the polymer, the measured dissociation forces are expected to be lower compared to the simple UPy-UPy dimer studied in the previous experiment.⁷³ This was confirmed for the supramolecular polymer, as a slight decrease of the dissociation force with increasing chain length was detected.

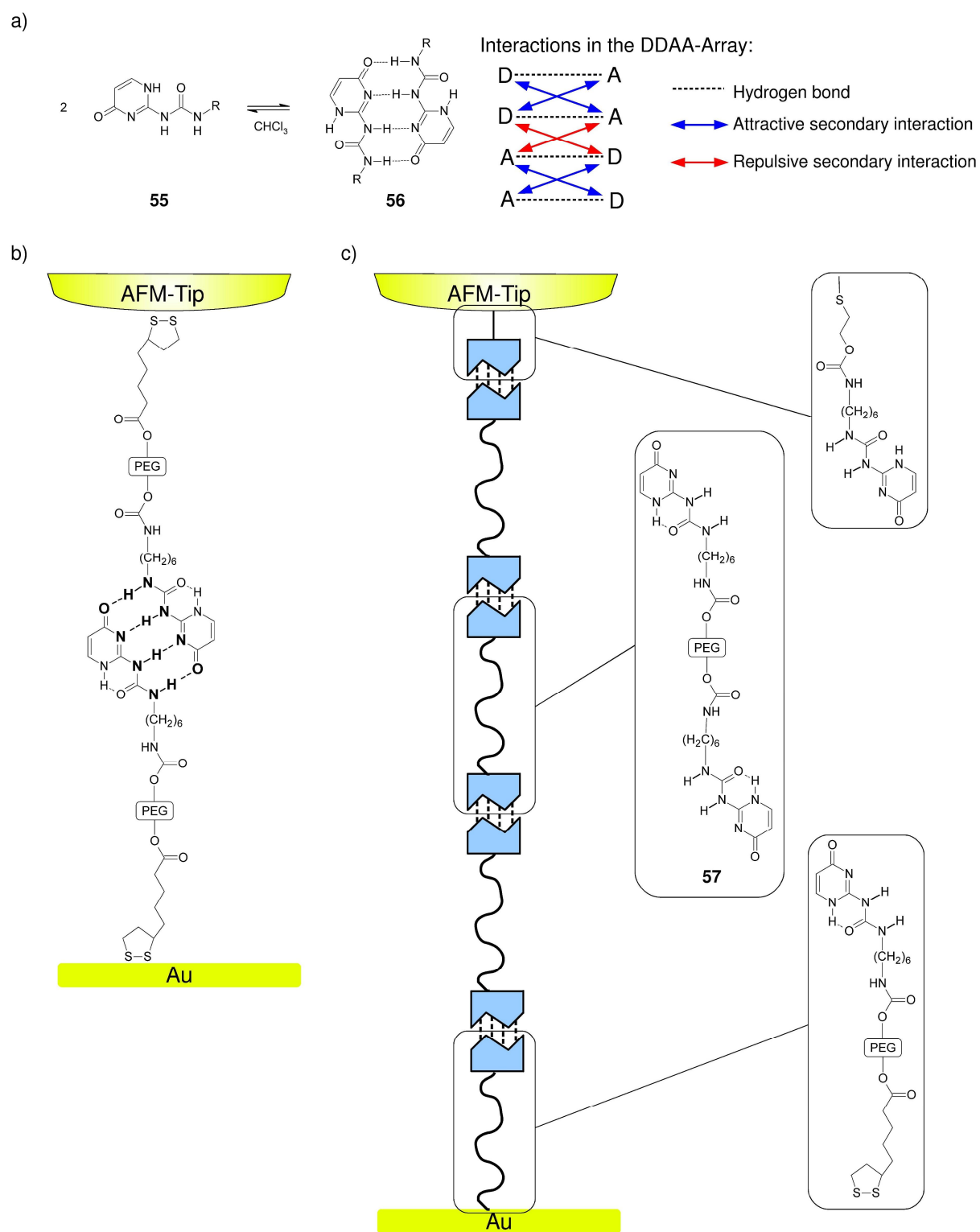


Figure 32: (a) Dimerization of 2-ureido-4(1*H*)-pyrimidinone. (b), (c) Setup of the SMFS experiments on the UPy dimers (b) and the supramolecular polymer (c).

In 2009, JAHNSHOFF *et al.* reported on the stretching of an oligomeric system that contains hydrogen-bonded tetra(urea)calix[4]arene capsules (Figure 33).⁷⁰ In this oligomer **58**, the capsules' halves are additionally connected by interlocked alkyl linkages (lines in Figure 33 b). Thus, the building blocks of the capsule can not be separated further than allowed by the alkyl linkages (without breaking the alkyl chains' covalent bonds, which is not the case in the measurements). The oligomer was attached to a gold-coated AFM tip *via* a thiolate (not shown in Figure 33). Upon approaching the cantilever to a positively charged surface, the carboxylate group at other end of the oligomer sticks to the substrate due to electrostatic interactions. This electrostatic attachment allowed stretching experiments on the molecule. When the cantilever was retracted from the surface, the stretching results in a consecutive dissociation of the hydrogen bonded capsules, while the covalent linkages of the capsules' halves stayed intact. In the corresponding AFM force curves in force spectroscopy experiments in a mixture of mesitylene and toluene (toluene serves as guest molecule for the capsule), characteristic sawtooth patterns with discrete rupture forces of $f^* = 30 - 100$ pN at loading rates of $r = 60 - 30\,000$ pN·s⁻¹ have been observed that could be assigned to subsequent capsule dissociation (Figure 33 c). But this assignment is not unambiguous due to a second process that needs to be considered: the stretching of the covalent linkages of the capsules proceeds *via* a sterically locked conformation, and overcoming of this intermediate states to completely stretched alkyl chains also results in distinct force steps. Because rupture forces due to hydrogen bond dissociation could not be clearly discriminated from forces required to overcome the locked conformation of the alkyl chains, a quantitative evaluation of the obtained data might be considered as inaccurate. Furthermore, a dependency of the dissociation forces on the number of non-covalently bound segments in the oligomer should be observed.⁷³ These factors impede the quantitative assessment of the stability of the supramolecular tetra(urea)calix[4]arene capsule from the obtained data.

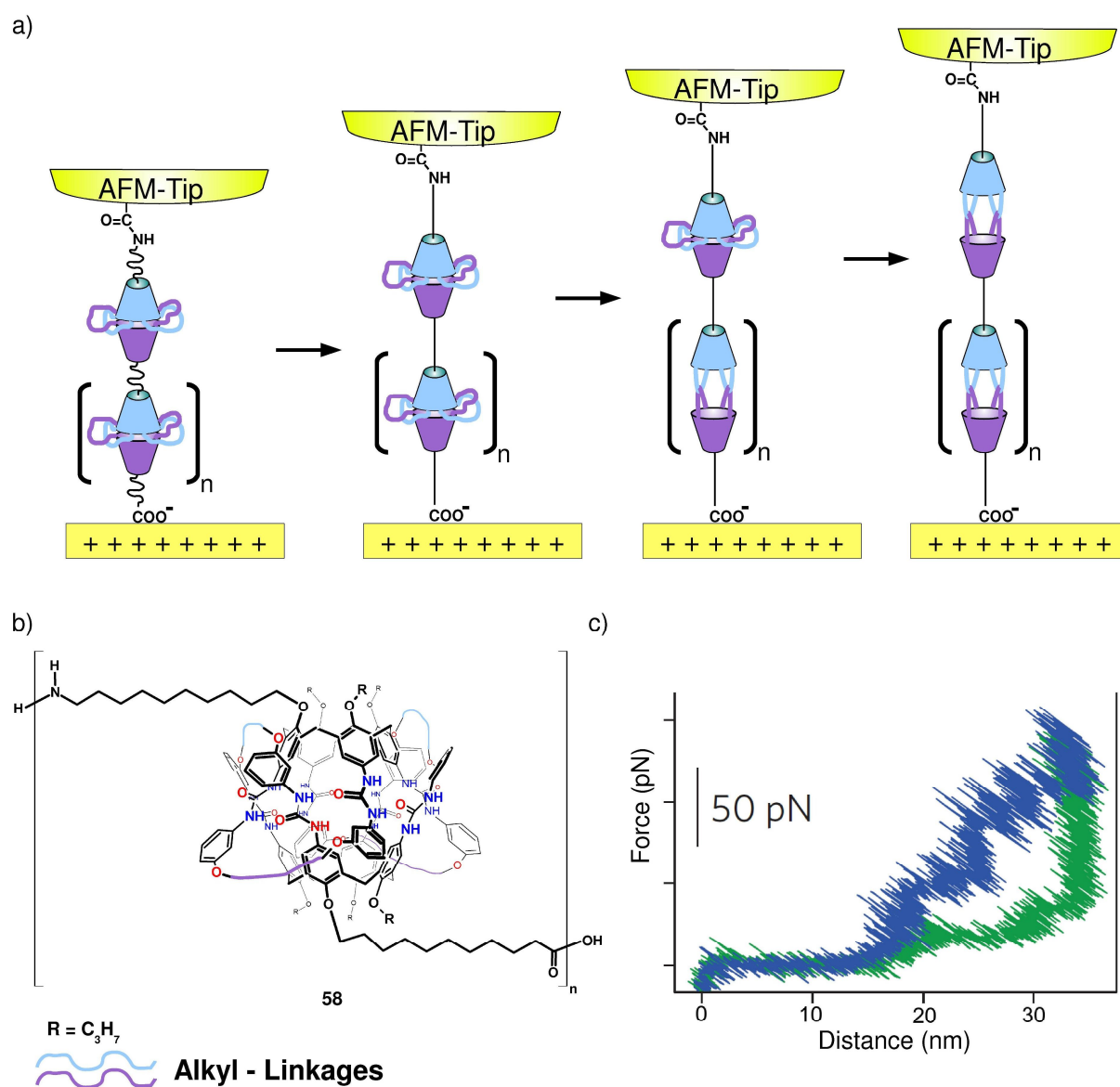


Figure 33: (a) Setup of a stretching experiment on oligo calix[4]arene catenanes – calix[4]arene dimers. (b) Structure of the oligomer. (c) Typical stretching (blue) and relaxation (green) curves obtained in force spectroscopy experiments (loading rate: $r = 300 \text{ pN}\cdot\text{s}^{-1}$).

3.4 Objective

Supramolecular capsules are an outstanding example of structures consisting of several building blocks connected by multiple non-covalent interactions. While the design and applications of supramolecular capsules are extensively studied, far less is known about their dynamic properties and no quantitative information on their mechanical stability has been provided. Single-molecule force spectroscopy makes important properties of molecules and supramolecular structures accessible, which can not be addressed by other methods. Providing quantitative data on the mechanical stability simultaneously with the kinetic and thermodynamic characteristics, this technique can afford a deeper understanding of bonding interactions in self-organized systems.

Within this study, single-molecule force spectroscopy is applied to a hydrogen bonded supramolecular capsule. To realize the experiment, the system should be composed of two main building blocks, which can be attached to the force sensor and a substrate. The heterodimeric capsule introduced by KOBAYASHI *et al.* is ideally suited for this purpose.²⁵ It consists of two cavitands connected by four hydrogen bonds between carboxylic acid and pyridyl groups. Furthermore, heterodimerization is highly selective and no isomers are formed. By functionalization of both cavitands at the *lower rim*, immobilization on surfaces can be achieved.

The setup of the single-molecule force spectroscopy experiment is shown in Figure 34. The tetra(carboxyl)cavitand is tethered to the cantilever via a flexible poly(ethylene glycol) linker (PEG linker), while the tetra(pyridyl)cavitand is immobilized at a gold substrate. The PEG linker adds steric freedom to the system that allows capsule formation to take place and reduces non-specific interaction. In addition, the use of PEG linkers yields characteristic stretching curves in SMFS experiments, facilitating discrimination of single-molecule from multiple dissociation events and the evaluation of molecular elasticities and single-molecule dissociation forces.

This experiment is aimed to yield detailed quantitative information on the stability of a supramolecular capsule under externally applied force and on the dynamics of the self-assembly process in the absence of external forces. The results will demonstrate that atomic force single-molecule force spectroscopy is an important and versatile tool for the characterization of non-covalent binding motifs and complex supramolecular structures.

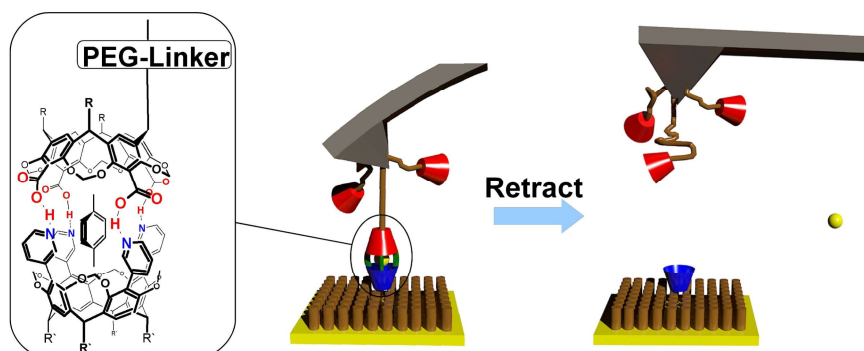


Figure 34: Setup of the SMFS experiments on a supramolecular capsule.

3.5 Results

3.5.1 Immobilization of the Building Blocks

The selective functionalization of the substrate and the cantilever is crucial for successful SMFS experiments. A well established method for the immobilization of cavitands on gold is the formation of self-assembled monolayers (SAMs) of thioether-footed cavitands.^{74,75} The tetra(pyridyl)cavitand **59** with four thioether moieties at the *lower rim* (Figure 35), which has been prepared in the group of Prof. Mattay, is suited for immobilization on a gold substrate. To obtain adsorbates of high quality, the self-assembly process is carried out at elevated temperatures (60 °C).

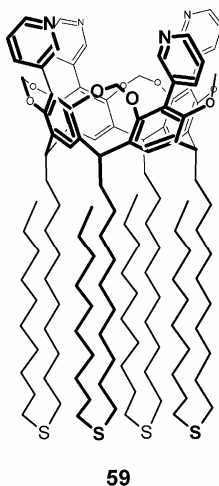


Figure 35: Structure of the tetra(pyridyl)cavitand **59**.

For single-molecule force spectroscopy experiments, the tetra(carboxyl)cavitand should be immobilized *via* a flexible poly(ethylene glycol) linker (PEG linker) to the cantilever, to add steric freedom to the system and allow complex formation to take place.⁷⁶ Figure 36 shows a schematic representation of the attachment. A PEG linker with one carboxylic acid group can be coupled to the amino-functionalized cantilever by amidation. The second terminal group of the heterobifunctional PEG should be attached *via* orthogonal coupling reaction to a tetra(carboxyl)cavitand with one appropriate reactive group at the *lower rim*. To prevent interaction with the tetra(carboxyl)cavitand, remaining free amino groups at the surface have to be blocked. Although the sequence of the coupling steps is not predetermined, a short sequence of reliable reactions on the cantilever surface is advantageous due to the high sensitivity of the cantilever towards mechanical damage. Therefore, the tetra(carboxyl)cavitand should be coupled to the PEG linker before the conjugate is attached to the cantilever.

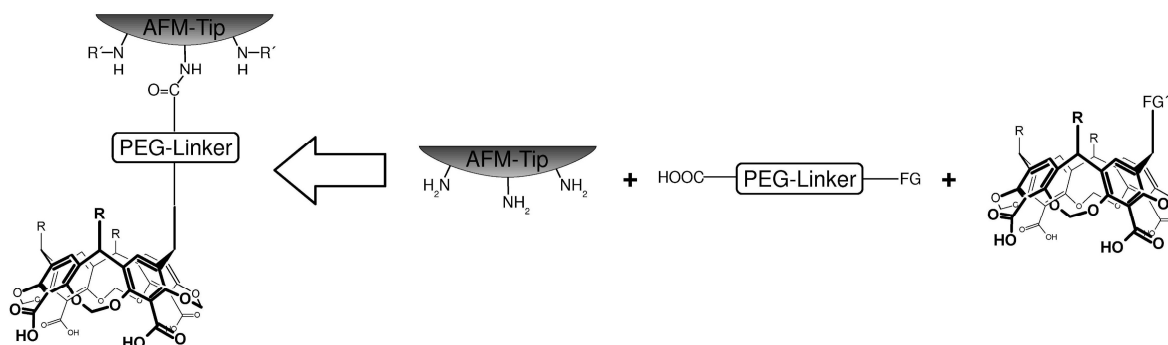
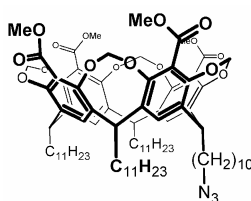


Figure 36: Scheme of the functionalization of the cantilever.

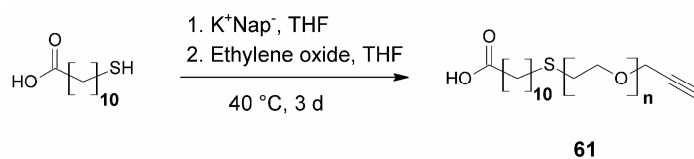
To realize the immobilization strategy, the synthesis of the tetra(carboxyl)cavitand **60** with one azido group at the *lower rim* was developed (Figure 37). Coupling of this building block to a PEG linker with a terminal alkyne should be possible by copper-catalyzed 1,3-dipolar cycloaddition of the azido group.⁷⁷



60

Figure 37: Structure of the cavitaand **60**.

Because a heterobifunctional PEG with one carboxyl group and one terminal alkyne is commercially not available, the linker **61** was prepared by anionic ring opening polymerization reaction of ethylene oxide and quenching the reaction by addition of propargyl bromide (Figure 38).



61

Figure 38: Synthesis of the heterobifunctional PEG linker **61**.

The synthesis of cavitaand **60** is shown in Figure 39. By condensation of resorcinol with a 1:3 mixture of 10-undecenal and dodecanal a statistical mixture of resorcin[4]arenes with up to four unsaturated alkyl chains was obtained. This mixture of compounds was brominated, the alkene moieties restored by debromination with zinc and the resorcin[4]arenes converted to the corresponding cavitaands by reaction with bromochloromethane.⁷⁸ The tetra(carboxyl)cavitaands **66** were obtained by lithiation and reaction with methyl chloroformate. Separation of the mixture of compounds was possible after introduction of the hydroxyl groups at the *lower rim* by hydroboration-oxidation. The tetra(carboxyl)cavitaand **67** with one hydroxyl group was isolated by column chromatography and converted into the methane sulfonate **68**. The azido group was introduced by substitution with sodium azide.

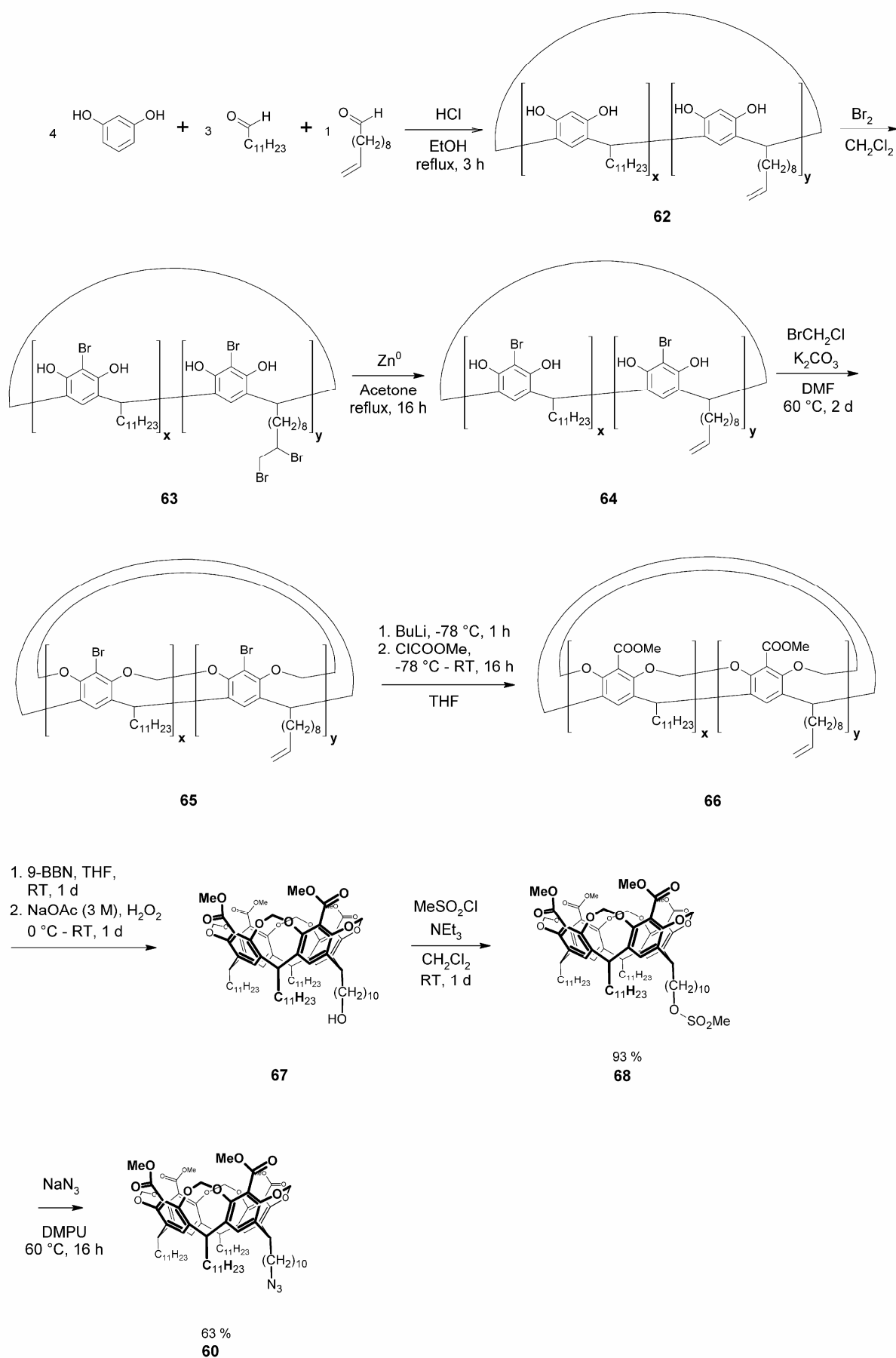


Figure 39: Synthesis of the tetra(carboxyl)cavitand **60** with one azido group.

Cavitand **60** was reacted with PEG linker **61** to get the conjugate, which was planned to be attached to the cantilever, but no evidence for successful cycloaddition was obtained. Therefore, a modified tetra(carboxyl)cavitand **73** with *para*-methoxybenzyl ester groups at the *upper rim* and one tetra(ethylene glycol) spacer at the *lower rim* was synthesized (Figure 40 and 41). While the *para*-methoxybenzyl ester groups can be cleaved under mild acidic conditions, the tetra(ethylene glycol) spacer should help to orient the azido group towards the very polar reaction medium used in the cycloaddition reaction.

The tetra(ethylene glycol) spacer **70** was obtained from undecynyl methane sulfonate and tetra(ethylene glycol) and subsequent conversion of the hydroxyl group to the methane sulfonate (Figure 40).

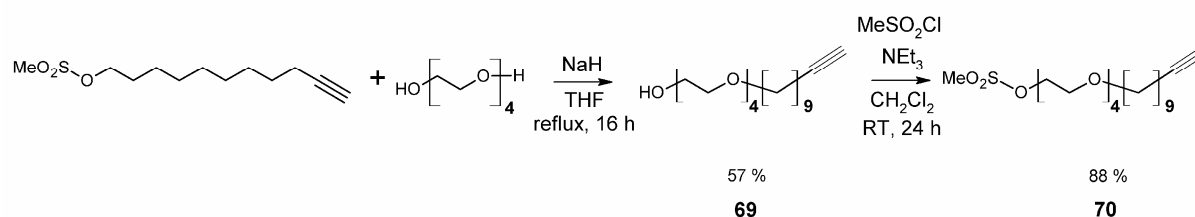


Figure 40: Synthesis of the spacer **70**.

Starting with the cavitand **60**, the methyl ester groups were substituted by *para*-methoxybenzyl ester groups, which are cleavable under mild acidic conditions (Figure 41). Copper-catalyzed 1,3-dipolar cycloaddition of the azido group to the terminal alkyne gave the methane sulfonate **72** which was reacted with sodium azide to yield the protected tetra(carboxyl)cavitand **73**.

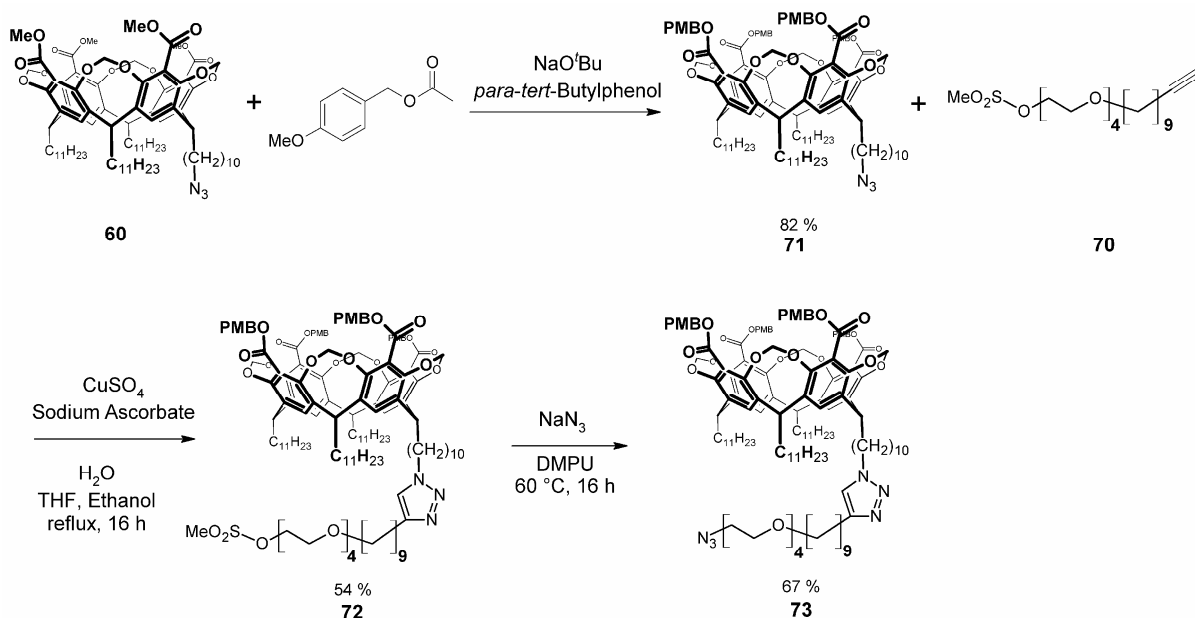
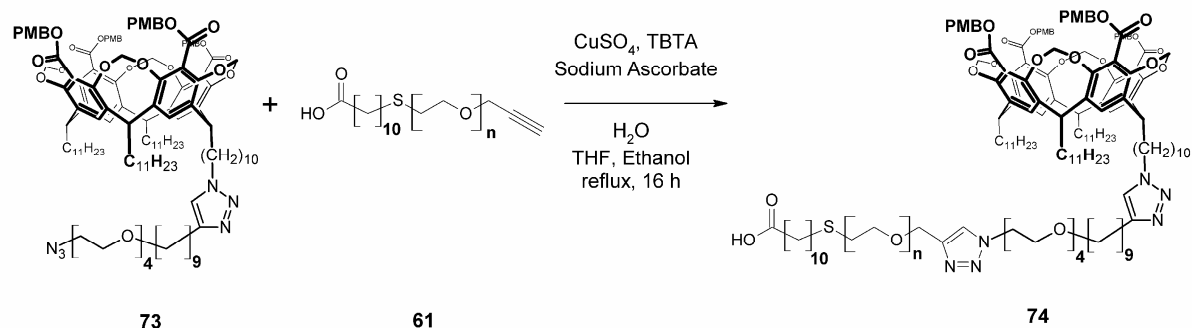


Figure 41: Preparation of the cavitand **73**.

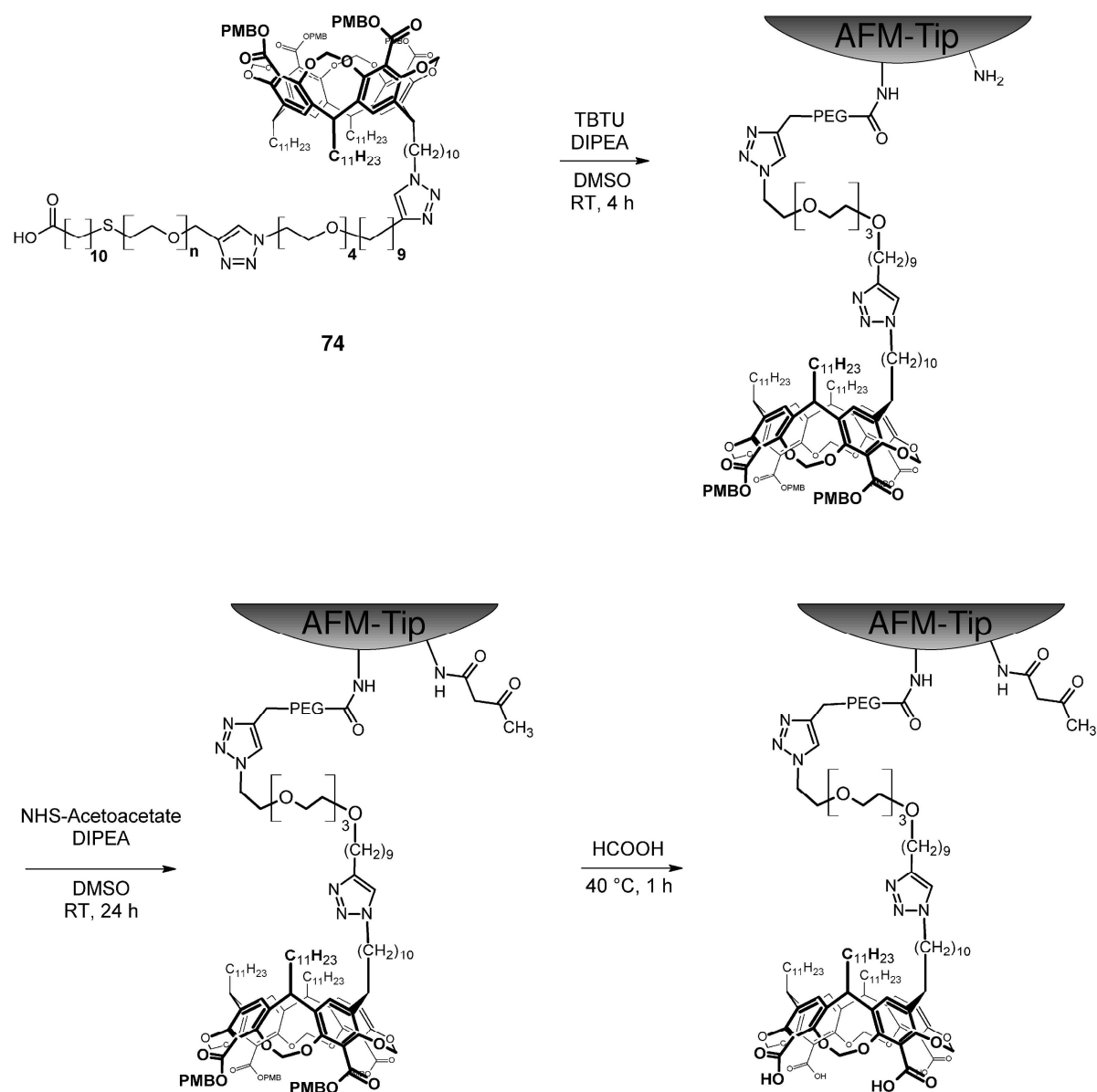
In contrast to the cavitand **60**, the azide **73** with the oligo(ethylene glycol) spacer was successfully reacted with the PEG linker **61** (Figure 42).



TBTA = tris-(benzyltriazolylmethyl)amine

Figure 42: Coupling of the cavitand **73** to the PEG linker **61**.

Attachment of the cavitand **74** to the amino-functionalized cantilever was accomplished using *O*-(Benzotriazol-1-yl)-*N,N,N',N'*-tetramethyluronium tetrafluoroborate (TBTU) as activating agent for the carboxylic acid group in dry DMSO (Figure 43). After blocking the remaining amino groups at the cantilever surface with *N*-hydroxysuccinimidyl acetoacetate, cantilever functionalization was completed by cleavage of the ester protecting groups.

**Figure 43:** Functionalization of the cantilever.

3.6 Single-Molecule Force Spectroscopy of Supramolecular Capsules

To get a first insight into the interactions between the capsules' halves by force spectroscopy, initial experiments were carried out using undiluted SAMs of the tetra(pyridyl)cavitand **59** on a gold substrate. A schematic representation of the experiment is shown in Figure 44. The tetra(carboxyl)cavitands are depicted as red bowls, while the tetra(pyridyl)cavitands immobilized at the gold substrate are represented by the blue bowls. All measurements are carried out in *para*-xylene which is encapsulated in the assembly (yellow ball).

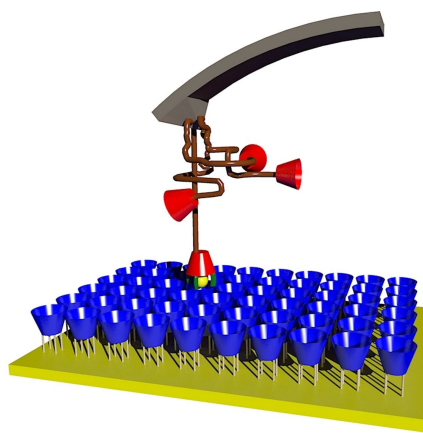


Figure 44: Scheme of the force spectroscopy experiments on an undiluted SAM of **59**.

Because of the high concentration of the tetra(pyridyl)cavitand at the substrate multiple interactions due to simultaneous formation of several supramolecular capsules were expected. This was actually observed, as reflected in a typical force curve shown in Figure 45. Several partially separated rupture events are detected, which sum up to a strong interaction between cantilever tip and substrate.

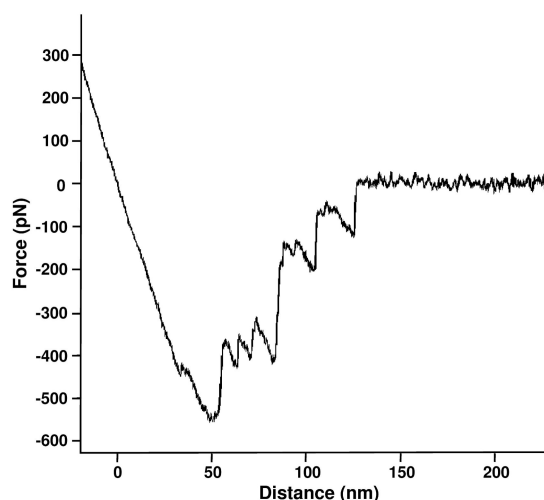


Figure 45: Typical force curve obtained in a force spectroscopy experiment using an undiluted SAM of **59**.

For the quantitative evaluation of the bonding interactions in the supramolecular capsule single-molecule force spectroscopy experiments are mandatory. Mixed SAMs containing alkylsulfides without functional groups can be used to realize a lower concentration at the substrate and reduce the binding activity between tip and sample.^{66,69,79} To prepare such diluted SAMs on gold, the substrates were placed in a solution (1 mM) of the cavitand **59** and decyl sulfide in a ratio of 1:100 at 60 °C for 10 h.^{74,75} In subsequent force spectroscopy experiments using the diluted SAM, a significant reduction of the binding activity was observed. While multiple rupture events were detected in all of the measurements on the undiluted SAM, the binding activity was significantly reduced using the diluted SAM (Figure 46). The typical force curve shown in Figure 46 a contains only one distinct force jump, which can be assigned to a rupture of a supramolecular capsule formed between a tetra(carboxyl)cavitand attached to the cantilever tip and a tetra(pyridyl)cavitand immobilized on the gold substrate. Characteristic non-linear force curves that could be assigned to the elastic stretching of the chain like polymer were observed and used to discriminate the specific single-molecule dissociation events from unspecific and multiple adhesion events. Furthermore, dissociation events were observed well separated from the surface (20 nm -80 nm), which simplifies identification and allows precise determination of the dissociation force. Force curves containing more than one minimum were discarded and not included in the data analysis.

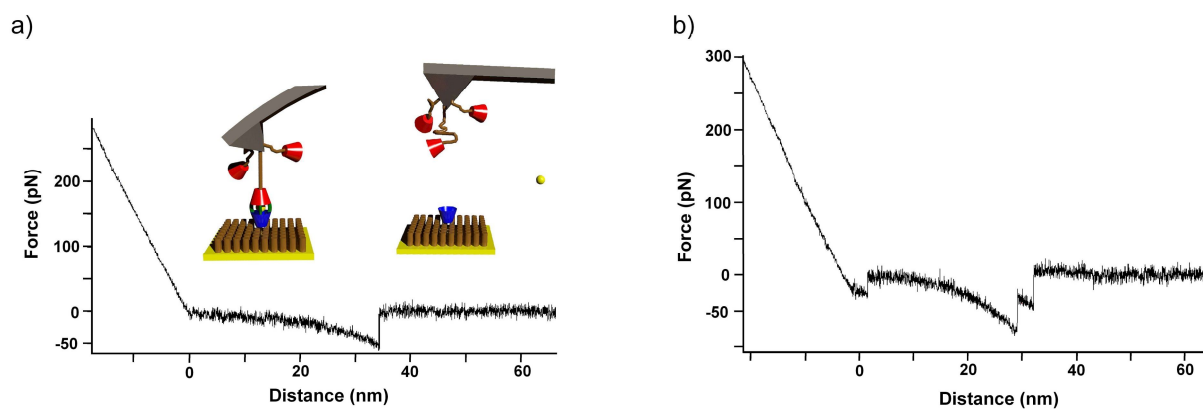


Figure 46: (a) Single-molecule dissociation event detected in a measurement on a diluted SAM of **59**. (b) Force curve containing a multiple adhesion event.

Plotting the detected dissociation forces in a histogram, a narrow distribution of forces characteristic for single-molecule force spectroscopy experiments was observed. To verify the specificity of the interaction, a control experiment was carried out (Figure 47). Addition of excess of free tetra(carboxyl)cavitand to the diluted SAM of the tetra(pyridyl)cavitand results in a strongly reduced binding activity between tip and sample due to effective blockage of the capsule formation between cantilever-bound tetra(carboxyl)cavitand and the tetra(pyridyl)cavitand.

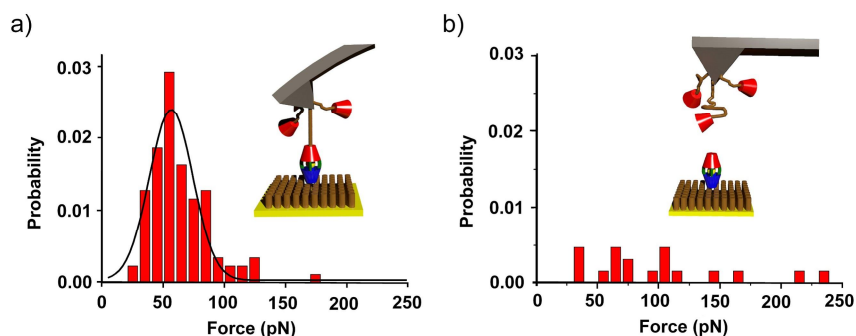


Figure 47: (a) Histogram of the dissociation forces of single heterodimeric capsules and Gaussian fit to the distribution. (b) Control experiment: Addition of free tetra(carboxyl)cavitand results in a strongly suppressed binding activity between tip and sample. Inset: Schematic representation of the competition experiment.

Further information about the mechanical stability of the supramolecular capsule was obtained from SMFS experiments carried out at different retract velocities. Single-molecule dissociation events were identified and the most probable dissociation forces obtained by fitting a Gaussian distribution to the histograms. Starting at $f^* = (39.1 \pm 4.1)$ pN at a loading rate of $r = 200$ pN·s⁻¹, the most probable dissociation rate increased to $f^* = (71 \pm 12)$ pN at a retract velocity of $v_r = 12\,600$ pN·s⁻¹. To relate the results to kinetic and thermodynamic properties of the system, the data were evaluated according to the theory of Bell and Evans.^{16,17} By plotting the most probable dissociation force f^* vs $\ln(r)$, the dissociation rate constant $k_{\text{off}}^0 = (0.14 \pm 0.14)$ s⁻¹ was obtained, that corresponds to an average bond lifetime of approximately $\tau \approx 7$ s (Figure 48). The molecular reaction length was determined to be $x_\beta = (0.560 \pm 0.076)$ nm. Assuming a typical fast association ($k_{\text{on}} = 1 \cdot 10^4$ M⁻¹·s⁻¹), the equilibrium constant of association can be estimated to be $K_a = 7.1 \cdot 10^4$ M⁻¹, yielding $\Delta G^0 = -27$ kJ·mol⁻¹.

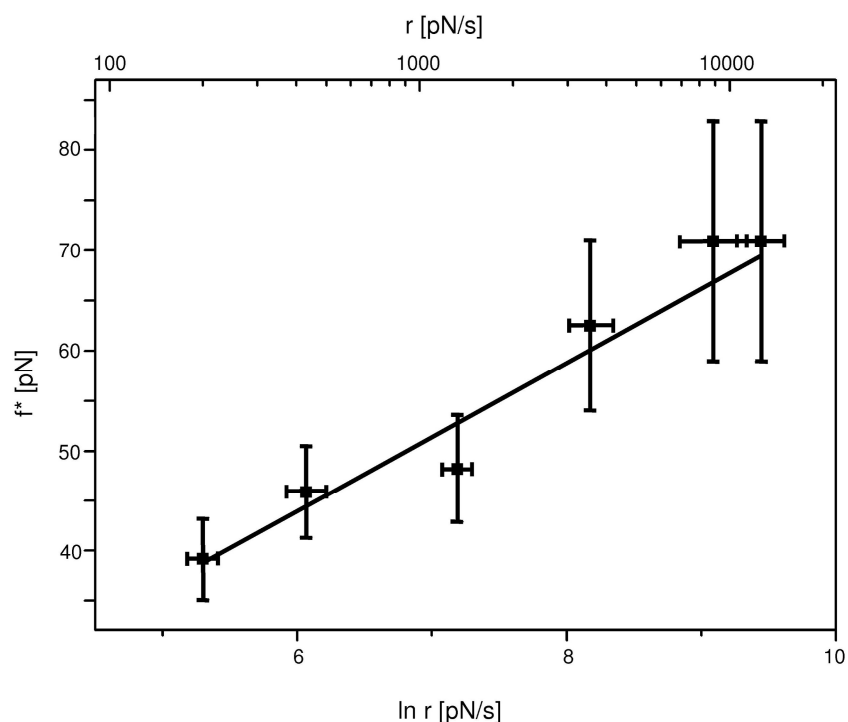


Figure 48: Plot and fitting analysis of the most probable dissociation forces against $\ln(r)$.

Compared to the tetra(urea)calix[4]arene capsules **48** and **51** and the cavitand capsule **54**, the heterodimeric aggregate analyzed in this study is expected to be less stable due to the lower number of hydrogen bonds connecting the building blocks. This is reflected in the dissociation rate constants: For the tetra(urea)calix[4]arene capsules **48** and **51**, which are held together by eight strong and eight weak hydrogen bonds, NMR and FRET measurements yielded dissociation rate constants of $k_{\text{off}} = 0.26 \text{ s}^{-1} - 5 \cdot 10^{-6} \text{ s}^{-1}$ ($\tau = 4 \text{ s} - 60 \text{ h}$), depending on the substituents at the urea and the *narrow rim*.^{54,55} The exchange of capsule subunits of the capsule **54**, which is stitched together by eight hydrogen bonds, was found to take place at exchange rates of $k = 1.9 \cdot 10^{-3} \text{ s}^{-1}$ ($\tau = 8.8 \text{ min}$) in toluene and at $k = 2.7 \cdot 10^{-6} \text{ s}^{-1}$ ($\tau = 100 \text{ h}$) in mesitylene in the presence of appropriate guest molecules.⁵⁶

The mechanical stability of the heterodimeric capsule analyzed in this study can be compared with the data obtained for the tetra(urea)calix[4]arene oligomer **58** and the UPy-UPy motif **56**. The dissociation forces of $f^* = 30 - 100 \text{ pN}$ at loading rates of $r = 60 - 30\,000 \text{ pN} \cdot \text{s}^{-1}$ measured for the oligomer **58** containing calix[4]arene capsules connected *via* eight strong and eight weak hydrogen bonds are in the same range as the dissociation forces of KOBAYASHI's capsule studied here.⁷⁰ However, the values determined in the stretching experiments on **58** might be influenced due to insufficient discrimination from the force steps resulting from the complete unfolding of a sterically locked conformation of the alkyl chains and might additionally be reduced because several non-covalently bound segments are stretched at the same time.⁷³ Therefore, our experimental setup seems to be better suited to determine the mechanical stability and the dynamics of the dissociation process of the supramolecular capsule quantitatively. The quadrupole hydrogen-bonded UPy-UPy motif **56** is mechanically more stable compared to KOBAYASHI's capsule. At similar loading rates, the most probable dissociation forces determined in SMFS experiments on **56** in hexadecane ($f^* = 174 \text{ pN}$ at $r = 11\,000 \text{ pN} \cdot \text{s}^{-1}$) exceed the values obtained for the capsule analyzed in this study.⁶⁴ The lifetimes of the associates ($\tau \approx 5 - 7 \text{ s}$ for the UPy-UPy dimer) are similar.

In conclusion, a reliable procedure for the immobilization of a tetra(carboxyl)cavitand at the cantilever and a tetra(pyridyl)cavitand at a gold substrate was developed that was the basis for successful AFM-SMFS experiments on a hydrogen-bonded capsule. Due to a suitable molecular design and experimental setup, quantitative evaluation of the interactions in this complex supramolecular structure could be realized. The obtained data are in good agreement with the values obtained from well-established ensemble measurements as well as SMFS experiments on hydrogen-bonded systems. The control of the mechanical stability of the supramolecular capsule **5** by appropriate guest molecules will be topic of further investigation. In contrast to other hydrogen-bonded motifs as the UPy-UPy dimer, the stability of this system could be precisely regulated, providing enhanced control over the self-assembly of supramolecular structures.

4 Summary

In this work, the synthesis and self-assembly dynamics of supramolecular capsules based on cavitands and calix[4]arenes is investigated.

Large supramolecular coordination cages have been prepared by metal-directed self-assembly of functionalized cavitands. To prevent intramolecular metal complexation and constrain the geometry of the potential self-assembled structures, the terpyridyl units were attached *via* rigid linkages to the cavitand basis. The tetra-(4-(2,2':6',2''-terpyridyl)-phenyl)-cavitand **40** was prepared from the boronic acid ester **39** and a tetraiodocavitand **38** by Suzuki-Miyaura-coupling reaction. Metal-directed self-assembly of **40** in the presence of Zn^{2+} ions yields the coordination cage **42** (Figure 49). ESI-MS confirms the hexameric structure of the aggregate. The NMR spectra indicate a high symmetry of the assembly, consistent with the proposed octahedral geometry.

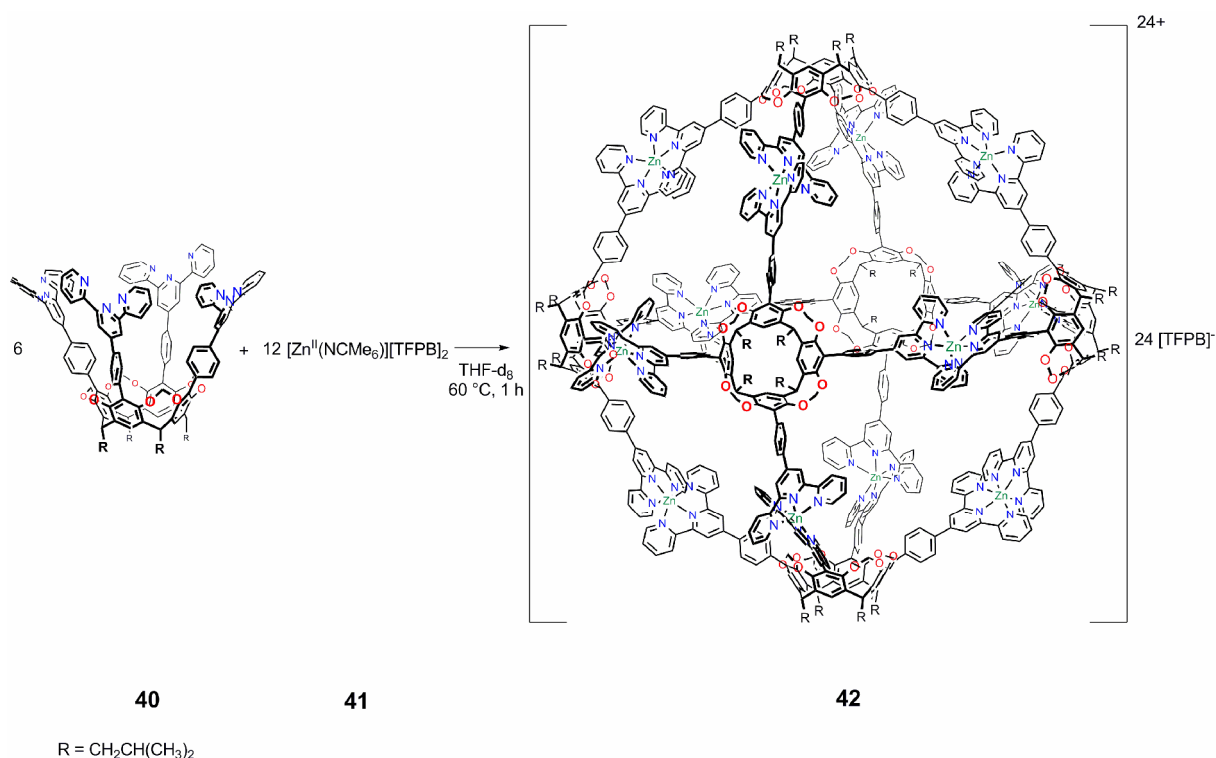
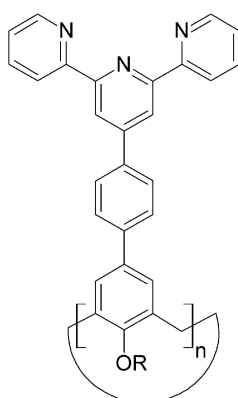


Figure 49: Synthesis of the coordination cage **42**.

The dimensions and form of the assembly were accessed by diffusion NMR spectroscopy and SAXS measurements, yielding a particle size of approximately 4 nm. These values are in very good agreement with the optimized structure obtained by Dr. Ralf Brodbeck using the semiempirical PM3 method. In the modeled structure, the cavitands are located at the apices of an octahedron with the edges of the platonic solid defined by Zn^{2+} ions coordinated by two terpyridine moieties. According to the calculations, the size of the assembly is 4.6 nm (distance between methyl groups of cavitands at opposite corners of the octahedron), while the inner cavity has a diameter of approximately 3 nm as determined using the program CAVER. The large cavity (volume $\approx 14 \text{ nm}^3$) is accessible for guest molecules *via* openings with a minimal diameter of 0.8 nm between adjacent bis-terpyridine complexes. Therefore, the interior of the coordination cage is large enough to encapsulate several bulky molecules simultaneously.

Calix[n]arenes **45 a**, **45 b** and **46** with four and five terpyridyl groups can be obtained by Suzuki-Miyaura coupling reaction of the boronic acid ester **39** with the tetrabromocalix[4]arenes **43 a** and **43 b** and the pentabromocalix[5]arene **44**, respectively (Figure 50).



45 a ($n = 4$, $R = n$ -Butyl)

45 b ($n = 4$, $R = \text{CH}_2\text{COOEt}$)

46 ($n = 5$, $R = \text{CH}_2\text{COO}^t\text{Bu}$)

Figure 50: Structure of the terpyridyl-substituted calix[4]arenes and calix[5]arene.

While the cavitand **40** self-assembles to the hexameric coordination cage **42**, the flexibility of the calix[n]arenes allows formation of various aggregates in the presence of Zn^{2+} ions. These results show, that the degree of preorganization has an important influence on the structures obtained in metal-directed self-assembly reactions. An interesting approach to prepare discrete coordination cages from the calix[n]arenes **45 a**, **45 b** and **46** is the addition of guest molecules of optimal size and shape to control the self-assembly process as demonstrated by SCHMITTEL *et al.*⁴⁴

The synthesis of the hexameric coordination cage **42** demonstrates, that functionalized cavitands can be used to obtain large metallocupramolecular capsules. By rigid attachment of terpyridyl units to the bowl-shaped cavitand moiety tetratopic ligands with an optimum geometry to self-assembly into cage structures have been obtained. Bis-terpyridine complexes of transition metal ions are especially well suited as stable connecting units, as indicated by successful detection of the intact coordination cage in ESI-MS. The encapsulation of guest molecules in the supramolecular assembly will be in the focus of future studies. Especially, the dependence of guest inclusion on the surrounding medium (polar, non-polar, fluoruous) is of interest for further applications. Simultaneous encapsulation of different bulky molecules and reactivity studies inside the coordination cage will give new insights into the processes in confined spaces. As terpyridine moieties functionalized at different positions are accessible, the coordination cage **42** can be considered as a prototype for a variety of metallocupramolecular capsules with a modified inner surface. The introduction of functional groups can lead to selective encapsulation and release as well as enhanced control of the reactivity of guest molecules.

In the second part of this work, the interactions in a hydrogen-bonded assembly have been studied using single-molecule force spectroscopy to evaluate the dynamics of the self-assembly process (Figure 51).

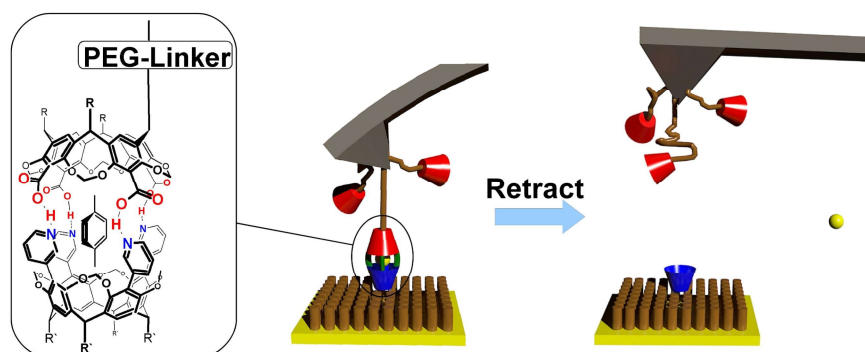


Figure 51: Setup of the single-molecule force spectroscopy experiment.

The immobilization of the building blocks of the hydrogen-bonded supramolecular capsule introduced by KOBAYASHI *et al.* in 2003 was the basis for successful SMFS experiments (Figure 52).²⁵ Therefore the tetra(carboxyl)cavitand **74** with acid-labile protecting groups and one azido group at the end of a tetra(ethylene glycol) spacer at the *lower rim* of the cavitand was synthesized. This cavitand was coupled to a heterobifunctional PEG linker obtained by anionic ring opening polymerization of ethylene oxide and quenching the reaction with propargyl bromide. The conjugate was immobilized at the amino-functionalized cantilever and the protecting groups cleaved under mild acidic conditions.

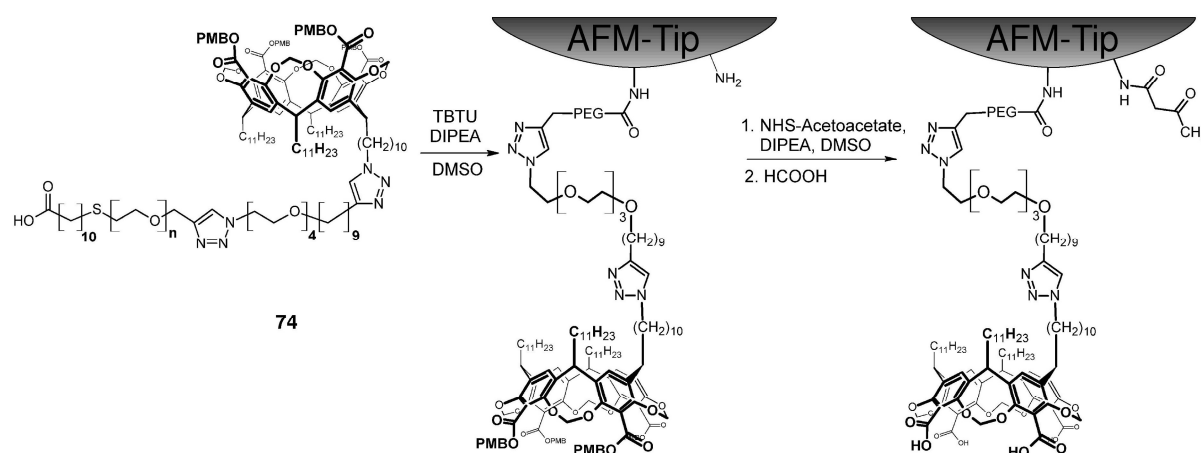


Figure 52: Functionalization of the cantilever with the tetra(carboxyl)cavitand **74**.

For initial force spectroscopy experiments, the thioether-footed tetra(pyridyl)cavitand **59** was immobilized as a SAM at a gold substrate. In the obtained force curves, strong adhesions between the cantilever tip and the sample were detected due to multiple interactions between the building blocks of the supramolecular capsule.

To reduce the binding activity between tip and sample, mixed SAMs containing the tetra(pyridyl)cavitand and excess of decyl sulfide were prepared. In the force spectroscopy experiments using this diluted SAMs, specific single-molecule dissociation events which could be assigned to the dissociation of single supramolecular capsules were observed. The specific curve form resulting from the stretching of the PEG linker was used to discriminate single-molecule dissociation events from unspecific or multiple adhesion events. Plotting the detected dissociation forces in a histogram, a typical distribution was obtained that could be fitted with a Gaussian distribution to determine the most probable dissociation force (f^*).

The specificity of the interaction was verified in a control experiment, where excess of free tetra(carboxyl)cavitand was added to the diluted SAM of the tetra(pyridyl)cavitand. In the force spectroscopy experiment, a strongly reduced binding activity was detected, because capsule formation between cantilever-bound tetra(carboxyl)cavitands and the tetra(pyridyl)cavitand was effectively blocked.

In dynamic single-molecule force spectroscopy experiments, the mechanical stability of the supramolecular capsules at different loading rates was investigated. In agreement with the model by Bell and Evans, the most probable dissociation forces f^* increased with the loading rate r (Figure 53). Quantitative evaluation of the obtained data according to this model allowed the determination of the kinetic dissociation rate $k_{\text{off}} = (0.14 \pm 0.14) \text{ s}^{-1}$, which corresponds to an average lifetime of the supramolecular capsule of 7 seconds. The molecular reaction length (width of the binding potential was determined to be $x_{\beta} = (0.560 \pm 0.076) \text{ nm}$. Assuming a typical fast association ($k_{\text{on}} = 1 \cdot 10^4 \text{ M}^{-1} \cdot \text{s}^{-1}$), the equilibrium constant of association was estimated to be $K_a = 7.1 \cdot 10^4 \text{ M}^{-1}$, yielding a value of $\Delta G^0 = -27 \text{ kJ} \cdot \text{mol}^{-1}$.

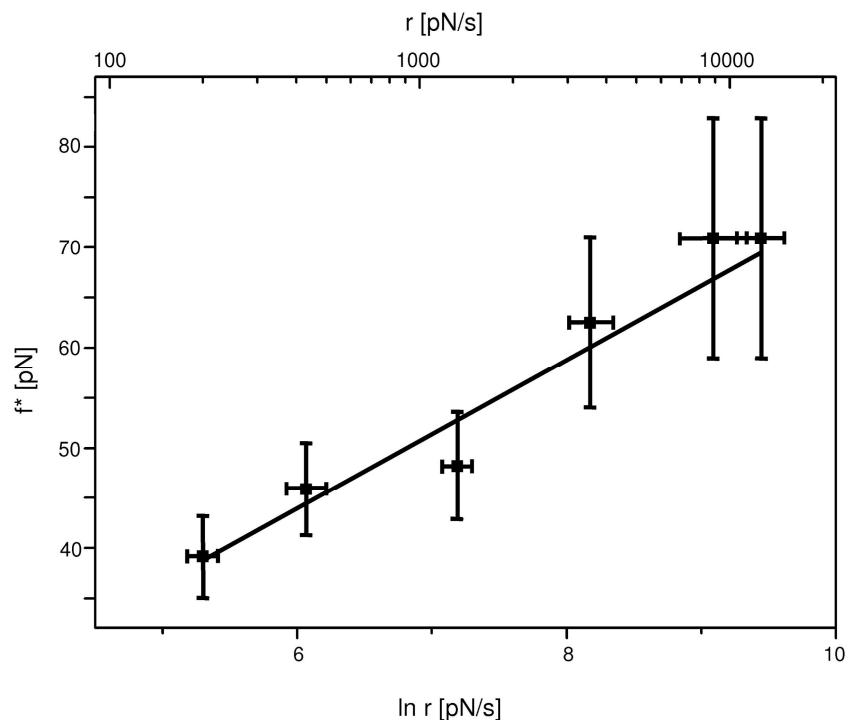


Figure 53: Plot of the most probable dissociation force f^* determined at different retract velocities v vs $\ln(r)$.

This investigation shows, that bonding interactions in complex supramolecular assemblies can be studied in detail using AFM-SMFS. In dynamic single-molecule force spectroscopy experiments the mechanical stability of a supramolecular capsule stitched together by four hydrogen bonds has been determined at different loading rates. Furthermore, the dynamics of the self-assembly process in the absence of external forces has been quantitatively accessed yielding the dissociation rate constant and an estimate of the equilibrium constant of association and the binding energy of the interaction. In further investigations, the influence of encapsulated guest molecules on the stability of the ternary system will be accessed.

This results demonstrate, that single-molecule force spectroscopy can provide important insights regarding the dynamic strength of supramolecular binding motifs. The consequent application of this technique will influence supramolecular design principles and the use of non-covalent interactions as construction elements.

5 References

- (1) a) Lehn, J. M. *Proc. Natl. Acad. Sci. USA* **2002**, *99*, 4763–4768. b) Lehn, J. M. *Angew. Chem.* **1988**, *100*, 91–116; *Angew. Chem. Int. Ed.* **1988**, *27*, 89–112.
- (2) Steed, J. W.; Atwood, J. L. *Supramolecular chemistry*, 2. ed.; Wiley, Chichester, **2009**.
- (3) Uraguchi, D.; Ueki, Y.; Ooi, T. *Science* **2009**, *326*, 120–123.
- (4) Cordier, P.; Tournilhac, F.; Soulie-Ziakovic, C.; Leibler, L. *Nature (London, U.K.)* **2008**, *451*, 977–980.
- (5) Schenning, A. P. H. J.; Meijer, E. W. *Chem. Comm.* **2005**, 3245–3258.
- (6) Lehn, J. M. *Chem. Soc. Rev.* **2007**, *36*, 151–160.
- (7) Rebek, J. *Angew. Chem.* **2005**, *117*, 2104–2115; *Angew. Chem., Int. Ed.* **2005**, *44*, 2068–2078.
- (8) Hof, F.; Craig, S. L.; Nuckolls, C.; Rebek, J. *Angew. Chem.* **2002**, *114*, 1556–1578; *Angew. Chem., Int. Ed.* **2002**, *41*, 1488–1508.
- (9) a) Yoshizawa, M.; Tamura, M.; Fujita, M. *Science* **2006**, *312*, 251–254. b) Fiedler, D.; Leung, D. H.; Bergman, R. G.; Raymond, K. N. *Acc. Chem. Res.* **2005**, *38*, 349–358. c) Mal, P.; Breiner, B.; Rissanen, K.; Nitschke, J. R. *Science* **2009**, *324*, 1697–1699. d) Pluth, M. D.; Bergman, R. G.; Raymond, K. N. *Science* **2007**, *316*, 85–88. e) Koblenz, T. S.; Wassenaar, J.; Reek, J. N. *Chem. Soc. Rev.* **2008**, *37*, 247–262. f) Fujita, M.; Tominaga, M.; Hori, A.; Therrien, B. *Acc. Chem. Res.* **2005**, *38*, 369–378. g) Vriezema, D. M.; Comellas Aragones, M.; Elemans, J. A. A. W.; Cornelissen, J. J. L. M.; Rowan, A. E.; Nolte, R. J. M. *Chem. Rev.* **2005**, *105*, 1445–1490. h) Yoshizawa, M.; Klosterman, J. K.; Fujita, M. *Angew. Chem.* **2009**, *121*, 3470–3490; *Angew. Chem., Int. Ed.* **2009**, *48*, 3418–3438.
- (10) Dalgarno, S. J.; Power, N. P.; Atwood, J. L. *Coord. Chem. Rev.* **2008**, *252*, 825–841.
- (11) a) Gianneschi, N. C.; Masar, M. S.; Mirkin, C. A. *Acc. Chem. Res.* **2005**, *38*, 825–837. b) Schneider, H. J. *Angew. Chem.* **2009**, *121*, 3982–4036; *Angew. Chem., Int. Ed.* **2009**, *121*, 3924–3977. c) Prins, L. J.; Reinhoudt, D. N.; Timmerman, P. *Angew. Chem.* **2001**, *113*, 2446–2492; *Angew. Chem., Int. Ed.* **2001**, *40*, 2382–2426.
- (12) Kienberger, F.; Ebner, A.; Gruber, H. J.; Hinterdorfer, P. *Acc. Chem. Res.* **2006**, *39*, 29–36.
- (13) Müller, D. J.; Dufrêne, Y. *Nat. Nanotechnol.* **2008**, *3*, 261–269.
- (14) a) Hugel, T.; Holland, N. B.; Cattani, A.; Moroder, L.; Seitz, M.; Gaub, H. E. *Science* **2002**, *296*, 1103–1106. b) Shi, W.; Giannotti, M. I.; Zhang, X.; Hempenius, M. A.; Schönherr, H.; Vancso, G. J. *Angew. Chem.* **2007**, *119*, 8552–8556; *Angew. Chem., Int. Ed.* **2007**, *46*, 8400–8404. c) Neuman, K. C.; Nagy, A. *Nat. Methods* **2008**, *5*, 491–505.

- (15) Janshoff, A.; Neizert, M.; Oberdörfer, Y.; Fuchs, H. *Angew. Chem.* **2000**, *112*, 3346–3374; *Angew. Chem., Int. Ed.* **2000**, *39*, 3213–3237.
- (16) Bell, G. I. *Science* **1978**, *200*, 618–627.
- (17) Evans, E.; Ritchie, K. *Biophys. J.* **1997**, *72*, 1541–1555.
- (18) Evans, E. *Annu. Rev. Biophys. Biomol. Struct.* **2001**, *30*, 105–128.
- (19) Cram, D. J.; Karbach, S.; Kim, Y. H.; Baczynskyj, L.; Kallemeyn, G. W. *J. Am. Chem. Soc.* **1985**, *107*, 2575–2576.
- (20) a) Botta, B.; Cassani, M.; D'Acquarica, I.; Subissati, D.; Zappia, G.; Delle Monache, G. *Curr. Org. Chem.* **2005**, *9*, 1167–1202. b) Timmerman, P.; Verboom, W.; Reinhoudt, D. N. *Tetrahedron* **1996**, *52*, 2663–2704.
- (21) Böhmer, V. *Angew. Chem.* **1995**, *107*, 785–818; *Angew. Chem., Int. Ed.* **1995**, *34*, 713–745.
- (22) Asfari, Z.; Böhmer, V.; Harrowfield, J.; Vicens, J. *Calixarenes 2001*; 1. ed., Kluwer Academic Publ., Dordrecht, **2001**.
- (23) a) Crisóstomo, F. R. P.; Lledó, A.; Shenoy, S. R.; Iwasawa, T.; Rebek, J. *J. Am. Chem. Soc.* **2009**, *131*, 7402–7410. b) Ruderisch, A.; Iwanek, W.; Pfeiffer, J.; Fischer, G.; Albert, K.; Schurig, V. *J. Chromatogr. A* **2005**, *1095*, 40–49. c) Baldini, L.; Casnati, A.; Sansone, F.; Ungaro, R. *Chem. Soc. Rev.* **2007**, *36*, 254–266.
- (24) Moran, J. R.; Ericson, J. L.; Dalcanale, E.; Bryant, J. A.; Knobler, C. B.; Cram, D. J. *J. Am. Chem. Soc.* **1991**, *113*, 5707–5714.
- (25) Kobayashi, K.; Ishii, K.; Sakamoto, S.; Shirasaka, T.; Yamaguchi, K. *J. Am. Chem. Soc.* **2003**, *125*, 10615–10624.
- (26) Kobayashi, K.; Ishii, K.; Yamanaka, M. *Chem. - Europ. J.* **2005**, *11*, 4725–4734.
- (27) Mogck, O.; Böhmer, V.; Vogt, W. *Tetrahedron* **1996**, *52*, 8489–8496.
- (28) Mogck, O.; Paulus, E. F.; Böhmer, V.; Thondorf, I.; Vogt, W. *Chem. Comm.* **1996**, 2533–2534.
- (29) Castellano, R. K.; Kim, B. H.; Rebek, J. *J. Am. Chem. Soc.* **1997**, *119*, 12671–12672.
- (30) a) Castellano, R. K.; Clark, R.; Craig, S. L.; Nuckolls, C.; Rebek, J. *Proc. Natl. Acad. Sci. USA* **2000**, *97*, 12418–12421. b) Castellano, R. K.; Rebek, J. *J. Am. Chem. Soc.* **1998**, *120*, 3657–3663. c) Castellano, R. K.; Rudkevich, D. M.; Rebek, J. *Proc. Natl. Acad. Sci. USA* **1997**, *94*, 7132–7137.
- (31) Steed, J. W.; Turner, D. R.; Wallace, K. J. *Core concepts in supramolecular chemistry and nanochemistry*, 1. ed., Wiley, Chichester, **2007**, pp. 107–170.
- (32) a) Fochi, F.; Jacopozzi, P.; Wegelius, E.; Rissanen, K.; Cozzini, P.; Marastoni, E.; Fisticaro, E.; Manini, P.; Fokkens, R.; Dalcanale, E. *J. Am. Chem. Soc.* **2001**, *123*, 7539–7552. b) Jacopozzi, P.; Dalcanale, E. *Angew. Chem.* **1997**, *109*, 665–667; *Angew. Chem., Int. Ed.* **1997**, *36*, 613–615.
- (33) a) Park, S. J.; Shin, D. M.; Sakamoto, S.; Yamaguchi, K.; Chung, Y. K.; Lah, M. S.; Hong, J. I. *Chem. - Europ. J.* **2005**, *11*, 235–241. b) Park, S. J.; Hong, J. I. *Chem. Comm.* **2001**, 1554–1555.

- (34) Fox, O. D.; Cookson, J.; Wilkinson, E. J.; Drew, M. G.; MacLean, E. J.; Teat, S. J.; Beer, P. D. *J. Am. Chem. Soc.* **2006**, *128*, 6990–7002.
- (35) Fox, O. D.; Drew, M. G.; Wilkinson, E. J.; Beer, P. D. *Chem. Comm.* **2000**, 391–392.
- (36) Fox, D. O.; Drew, M. G. B.; Beer P. D. *Angew. Chem.* **2000**, *112*, 139–144; *Angew. Chem., Int. Ed.* **2000**, *112*, 135–140.
- (37) Ugono, O.; Moran, J. P.; Holman, K. T. *Chem. Comm.* **2008**, 1404–1406.
- (38) Constable, E. C. *Chem. Soc. Rev.* **2007**, *36*, 246–253.
- (39) Schubert, U. S.; Hofmeier, H.; Newkome, G. R. *Modern terpyridine chemistry*; 1. ed., Wiley-VCH, Weinheim, **2006**.
- (40) Dumitru, F.; Petit, E.; van der Lee, A.; Barboiu, M. *Eur. J. Inorg. Chem.* **2005**, 4255–4262.
- (41) Garcia, A. M.; Bassani, D. M.; Lehn, J. M.; Baum, G.; Fenske, D. *Chem. - Europ. J.* **1999**, *5*, 1234–1238.
- (42) Schmittel, M.; He, B. *Chem. Comm.* **2008**, 4723–4725.
- (43) Schmittel, M.; Kalsani, V.; Mal, P.; Bats, J. W. *Inorg. Chem.* **2006**, *45*, 6370–6377.
- (44) Schmittel, M.; He, B.; Mal, P. *Org. Lett.* **2008**, *10*, 2513–2516.
- (45) Aspley, C. J.; Williams, J. A. *New J. Chem.* **2001**, *25*, 1136–1147.
- (46) a) Buschmann, W. E.; Miller, J. S. *Chem. - Europ. J.* **1998**, *4*, 1731–1737. b) Brookhart, M.; Grant, B.; Volpe, A. F. *Organometallics* **1992**, *11*, 3920–3922. c) Nishida, H.; Tadaka, N.; Yoshimura, M.; Sonoda, T.; Kobayashi, H. *Bull. Chem. Soc. Jpn.* **1984**, *57*, 2600–2604.
- (47) Cohen, Y.; Avram, L.; Frish, L. *Angew. Chem.* **2005**, *117*, 524–560; *Angew. Chem., Int. Ed.* **2005**, *44*, 520–554.
- (48) Glatter, O. *J. Appl. Crystallogr.* **1979**, *12*, 166–175.
- (49) a) Svergun, D. I. *J. Appl. Crystallogr.* **1992**, *25*, 495–503. b) Svergun, D. I. *Biophys. J.* **1999**, *76*, 2879–2886. c) Svergun, D. I. *J. Appl. Crystallogr.* **1991**, *24*, 485–492. d) Semeyukav, A. V.; Svergun, D. I. *J. Appl. Crystallogr.* **1991**, *24*, 537–540.
- (50) Stewart, J. J. *J. Comp. Chem.* **1989**, *13*, 157–158.
- (51) Damborsky, J.; Petřek, P.; Banáš, P.; Otyepka, M. *Biotechnol. J.* **2007**, *2*, 62–67.
- (52) Liu, J. M.; Tonigold, M.; Bredenkötter, B.; Schröder, T.; Mattay, J.; Volkmer, D. *Tetrahedron Lett.* **2009**, *50*, 1303–1306.
- (53) Yoshizawa, M.; Klosterman, J. K.; Fujita, M. *Angew. Chem.* **2009**, *121*, 3470–3490; *Angew. Chem., Int. Ed.* **2009**, *48*, 3418–3438.
- (54) Mogck, O.; Pons, M.; Böhmer, V.; Vogt, W. *J. Am. Chem. Soc.* **1997**, *119*, 5706–5712.
- (55) Castellano, R. K.; Craig, S. L.; Nuckolls, C.; Rebek, J. *J. Am. Chem. Soc.* **2000**, *122*, 7876–7882.
- (56) Barrett, E. S.; Dale, T. J.; Rebek, J. *J. Am. Chem. Soc.* **2007**, *129*, 8818–8824.
- (57) a) Binnig, G.; Quate, C. F.; Gerber, C. *Phys. Rev. Lett.* **1986**, *56*, 930. b) Drake, B.; Prater, C. B.; Weisenhorn, A. L.; Gould, S. A.; Albrecht, T. R.; Quate, C. F.; Cannell, D. S.; Hansma, H. G.; Hansma, P. K. *Science* **1989**, *243*, 1586–1589.

- (58) Meyer, G.; Amer, N. M. *Appl. Phys. Lett.* **1988**, *53*, 1045–1047.
- (59) Beyer, M. K.; Clausen-Schaumann, H. *Chem. Rev.* **2005**, *105*, 2921–2948.
- (60) Hutter, J. L.; Bechhoefer, J. *Rev. Sci. Instrum.* **1993**, *64*, 1868–1873.
- (61) Arrhenius, S. *Z. Phys. Chem.* **1889**, *4*, 226–248.
- (62) Fuhrmann, A.; Anselmetti, D.; Ros, R.; Getfert, S.; Reimann, P. *Phys. Rev. E* **2008**, *77*, 31912.
- (63) Zou, S.; Schönherr, H.; Vancso, G. J. *J. Am. Chem. Soc.* **2005**, *127*, 11230–11231.
- (64) Zou, S.; Schönherr, H.; Vancso, G. J. *Angew. Chem.* **2005**, *117*, 978–981; *Angew. Chem., Int. Ed.* **2005**, *44*, 956–959.
- (65) a) Zhang, Y.; Liu, C.; Shi, W.; Wang, Z.; Dai, L.; Zhang, X. *Langmuir* **2007**, *23*, 7911–7915. b) Ray, C.; Brown, J. R.; Kirkpatrick, A.; Akhremitchev, B. B. *J. Am. Chem. Soc.* **2008**, *130*, 10008–10018. c) Zhang, Y.; Yu, Y.; Jiang, Z.; Xu, H.; Wang, Z.; Zhang, X.; Oda, M.; Ishizuka, T.; Jiang, D.; Chi, L.; Fuchs, H. *Langmuir* **2009**, *25*, 6627–6632. d) Kudera, M.; Eschbaumer, C.; Gaub, H. E.; Schubert, U. S. *Adv. Funct. Mat.* **2003**, *13*, 615–620. e) Conti, M.; Falini, G.; Samori, B. *Angew. Chem.* **2000**, *112*, 221–224; *Angew. Chem., Int. Ed.* **2000**, *39*, 215–218.
- (66) Eckel, R.; Ros, R.; Decker, B.; Mattay, J.; Anselmetti, D. *Angew. Chem.* **2005**, *117*, 489–492 *Angew. Chem., Int. Ed.* **2005**, *44*, 484–488.
- (67) Schäfer, C.; Eckel, R.; Ros, R.; Mattay, J.; Anselmetti, D. *J. Am. Chem. Soc.* **2007**, *129*, 1488–1489.
- (68) Anselmetti, D.; Bartels, F. W.; Becker, A.; Decker, B.; Eckel, R.; McIntosh, M.; Mattay, J.; Plattner, P.; Ros, R.; Schäfer, C.; Sewald, N. *Langmuir* **2008**, *24*, 1365–1370.
- (69) Schäfer, C.; Decker, B.; Letzel, M.; Novara, F.; Eckel, R.; Ros, R.; Anselmetti, D.; Mattay, J. *Pure Appl. Chem.* **2006**, *78*, 2247–2259.
- (70) Janke, M.; Rudzevich, Y.; Molokanova, O.; Metzroth, T.; Mey, I.; Diezemann, G.; Marszalek, P. E.; Gauss, J.; Böhmer, V.; Janshoff, A. *Nat. Nanotechnol.* **2009**, *4*, 225–229.
- (71) Beijer, F. H.; Sijbesma, R. P.; Kooijman, H.; Spek, A. L.; Meijer, E. W. *J. Am. Chem. Soc.* **1998**, *120*, 6761–6769.
- (72) Söntjens, S. H. M.; Sijbesma, R. P.; van Genderen, M. H. P.; Meijer, E. W. *J. Am. Chem. Soc.* **2000**, *122*, 7487–7493.
- (73) Williams, P.; Evans, E. in *Physics of bio molecules and cells*, Ecoles des Houches d'Eté LXXV (Eds. Julicher, F.; Ormos, P.; David, F.; Flyvbjerg, H.), 1. ed., Springer: Berlin, **2002**, pp 147–203.
- (74) van Velzen, E. U. T.; Engbersen, J. F. J.; Lange, P. J. de; Mahy, J. W. G.; Reinhoudt, D. N. *J. Am. Chem. Soc.* **1995**, *117*, 6853–6862.
- (75) Schönherr, H.; Vancso, G. J.; Huisman, B.-H.; van Veggel, F. C. J. M.; Reinhoudt, D. N. *Langmuir* **1999**, *15*, 5541–5546.
- (76) Hinterdorfer, P.; Baumgartner, W.; Gruber, H. J.; Schilcher, K.; Schindler, H. *Proc. Natl. Acad. Sci. USA* **1996**, *93*, 3477–3481.

- (77) Rostovtsev, V. V.; Green, L. G.; Fokin, V. V.; Sharpless, K. B. *Angew. Chem.* **2002**, *114*, 2708–2711; *Angew. Chem., Int. Ed.* **2002**, *41*, 2596–2597.
- (78) a) Bryant, J. A.; Blanda, M. T.; Vincenti, M.; Cram, D. J. *J. Am. Chem. Soc.* **1991**, *113*, 2167–2172. b) Huisman, B. H.; Rudkevich, D. M.; Farran, A.; Verboom, W.; van Veggel, F.; Reinhoudt, D. N. *Eur. J. Org. Chem.* **2000**, 269–274.
- (79) a) Gilbert, Y.; Deghorain, M.; Wang, L.; Xu, B.; Pollheimer, P. D.; Gruber, H. J.; Errington, J.; Hallet, B.; Haulot, X.; Verbelen, C.; Hols, P.; Dufrene, Y. F. *Nano Lett.* **2007**, *7*, 796–801. b) Schmitt, L.; Ludwig, M.; Gaub, H. E.; Tampé, R. *Biophys. J.* **2000**, *78*, 3275–3285.

6 Appendix

6.1 Glossary

AFM	Atomic Force Microscope
AFM-SMFS	Atomic Force Single-Molecule Force Spectroscopy
BuLi	Butyllithium
DFS-SMFS	Dynamic Force Single-Molecule Force Spectroscopy
DIPEA	<i>N,N</i> -Diisopropylethylamine
DMF	<i>N,N</i> -Dimethylformamide
DMPU	1,3-Dimethyl-3,4,5,6-tetrahydro-2(1 <i>H</i>)-pyrimidinone
DMSO	Dimethyl sulfoxide
dppp	1,3-Bis(diphenylphosphino)propane
ESI-MS	Electrospray Ionization Mass Spectrometry
EtOH	Ethanol
FRET	Förster Resonance Energy Transfer
HETTAP	Heteroleptic terpyridine and phenanthroline aggregation
NaOAc	Sodium acetate
Nap ⁻	Naphthalinide
NHS-acetoacetate	<i>N</i> -Hydroxysuccinimidyl acetoacetate
NMR	Nuclear Magnetic Resonance
NOE	Nuclear Overhauser Effect
PEG	Poly(ethylene glycol)
PMBO	<i>para</i> -Methoxybenzyl
RT	Room temperature
SAM	Self-Assembled Monolayer
SAXS	Small Angle X-Ray Scattering
SMFS	Single-Molecule Force Spectroscopy
TBTA	Tris-(benzyltriazolylmethyl)amine
TBTU	<i>O</i> -(Benzotriazol-1-yl)- <i>N,N,N',N'</i> -tetramethyluronium tetrafluoroborate
TFPB	Tetrakis-(3,5-bis-(trifluoromethyl)-phenyl)-borate
THF	Tetrahydrofuran
UPy	2-Ureido-4(1 <i>H</i>)-pyrimidinone

6.2 List of Original Publications

1. „*Single-Molecule Force Spectroscopy of Supramolecular Heterodimeric Capsules.*”
Tobias Schröder, Thomas Geisler, Björn Schnatwinkel, Dario Anselmetti, Jochen Mattay, *submitted*.
2. „*Synthesis of terpyridine-substituted calix[n]arenes.*”
Junmin Liu, Markus Tonigold, Björn Bredenkötter, Tobias Schröder, Jochen Mattay, Dirk Volkmer, *Tetrahedron Lett.* **2009**, 50, 1303–1306.
3. „*A self-assembling metallosupramolecular cage based on cavitand–terpyridine subunits.*”
Tobias Schröder, Ralf Brodbeck, Matthias C. Letzel, Andreas Mix, Björn Schnatwinkel, Markus Tonigold, Dirk Volkmer, Jochen Mattay, *Tetrahedron Lett.* **2008**, 49, 5939.